An oomycete effector targets a plant RNA helicase involved in root development and defense

Laurent Camborde, Andrei Kiselev, Michiel Pel, Aurélie Le Ru, Alain Jauneau, Cécile Pouzet, Bernard Dumas, Elodie Gaulin

Research

New Phytologist

An oomycete effector targets a plant RNA helicase involved in root development and defense

Laurent Camborde[1], Andrei Kiselev[1], Michiel J. C. Pel[1], Aurélie Le Ru[2], Alain Jauneau[2], Cécile Pouzet[2], Bernard Dumas[1] and Elodie Gaulin[1]

[1]Laboratoire de Recherche en Sciences Végétales (LRSV), Université de Toulouse, CNRS, UPS, Toulouse INP, Auzeville-Tolosane 31320, France; [2]Plateforme d'Imagerie FRAIB-TRI, Université de Toulouse, CNRS, Auzeville-Tolosane 31320, France

Author for correspondence:
Elodie Gaulin
Email: gaulin@lrsv.ups-tlse.fr

Received: *12 July 2021*
Accepted: *3 December 2021*

New Phytologist (2022) **233:** 2232–2248
doi: 10.1111/nph.17918

Key words: *Aphanomyces*, effectors, *Medicago*, MtRH10, nucleolar stress, oomycete, plant development, RNA-helicase.

Summary

- Oomycete plant pathogens secrete effector proteins to promote disease. The damaging soilborne legume pathogen *Aphanomyces euteiches* harbors a specific repertoire of Small Secreted Protein effectors (AeSSPs), but their biological functions remain unknown. Here we characterize AeSSP1256.
- The function of AeSSP1256 is investigated by physiological and molecular characterization of *Medicago truncatula* roots expressing the effector. A potential protein target of AeSSP1256 is identified by yeast-two hybrid, co-immunoprecipitation, and fluorescent resonance energy transfer–fluorescence lifetime imaging microscopy (FRET–FLIM) assays, as well as promoter studies and mutant characterization.
- AeSSP1256 impairs *M. truncatula* root development and promotes pathogen infection. The effector is localized to the nucleoli rim, triggers nucleoli enlargement and downregulates expression of *M. truncatula* ribosome-related genes. AeSSP1256 interacts with a functional nucleocytoplasmic plant RNA helicase (MtRH10). AeSSP1256 relocates MtRH10 to the perinucleolar space and hinders its binding to plant RNA. MtRH10 is associated with ribosome-related genes, root development and defense.
- This work reveals that an oomycete effector targets a plant RNA helicase, possibly to trigger nucleolar stress and thereby promote pathogen infection.

Introduction

Plant pathogens alter host cellular physiology to promote their own proliferation by producing effector proteins that interact with plant molecular targets. Previous studies have indicated large variations in the effector repertoire of plant pathogens, suggesting that a large number of molecular mechanisms are targeted by these effectors (He *et al.*, 2020).

Oomycetes constitute a large phylum and include important filamentous eukaryotic pathogens, many of which cause disease in plants or animals (van West & Beakes, 2014; Kamoun *et al.*, 2015). The presence of conserved motifs in some oomycete sequences has allowed the computational prediction of many candidate effectors in the oomycete genome (Haas *et al.*, 2009; McGowan & Fitzpatrick, 2017; Tabima & Grünwald, 2019). There is increasing evidence that the plant nucleus is an important compartment for effector function, mainly because of the large portfolio of putative nucleus-targeting effectors predicted in oomycete genomes (Schornack *et al.*, 2010; Stam *et al.*, 2013; Song *et al.*, 2015; Zhang *et al.*, 2015; Wang *et al.*, 2019). Accordingly, different mechanisms of action at the nuclear level have been reported, including alteration of gene transcription (Song *et al.*, 2015; Wirthmueller *et al.*, 2018; He *et al.*, 2019), mis-localization of transcription factors (McLellan *et al.*, 2013), suppression of RNA silencing by inhibition of siRNA accumulation (Xiong *et al.*, 2014; Qiao *et al.*, 2015), and plant DNA damage (Ramirez-Garcés *et al.*, 2016; Camborde *et al.*, 2019). However, only a small number of oomycete effectors have been assigned a specific function.

Aphanomyces euteiches, the causal agent of pea root rot disease, is a major pathogen that affects crop and forage legumes and naturally infects the model legume *Medicago truncatula* (Gaulin *et al.*, 2007). The severity of symptoms observed upon exposure of natural *M. truncatula* lines to the pathogen showed a continuous gradient, indicating that the interaction is quantitative, ranging from a relative resistance phenotype to a high susceptibility phenotype (Djébali *et al.*, 2009; Jacquet & Bonhomme, 2020). Among *M. truncatula,* the susceptible F83005.5 line developed symptoms within a few days and commonly died within 3 wk, whereas the A17-Jemalong partially resistant line displayed retarded growth and a delay in the appearance of symptoms (Djébali *et al.*, 2009; Jacquet & Bonhomme, 2020). Partial resistance to *A. euteiches* in *M. truncatula* and in pea has been shown to be controlled by numerous quantitative trait loci (QTLs) whose effects on the disease range from minor to major (Hamon *et al.*, 2013; Bonhomme *et al.*, 2014, 2019; Desgroux *et al.*,

2018). No fully resistant lines have been reported, and the observed partial resistance is commonly linked to the development of a large number of roots and lateral roots (Bonhomme *et al.*, 2014, 2019; Badis *et al.*, 2015; Desgroux *et al.*, 2018).

In our recent work, we have combined transcriptomics and genomics analyses to identify *A. euteiches* pathogenic determinants. We identified a new class of effectors of > 290 Small Secreted Proteins (AeSSPs) specifically found in *A. euteiches* (Gaulin *et al.*, 2018). These AeSSPs contain a predicted N-terminus signal peptide, are < 300 residues in length, and are devoid of any functional annotations. Many AeSSPs contain a predicted nuclear localization signal (NLS), suggesting that these are probably active within the host nucleus. Screening to identify plant nuclear-localized *A. euteiches* effectors that can promote *Phytophthora capsici* infection led to the identification of AeSSP1256. This effector, which is upregulated during early colonization of *M. truncatula* roots, presented a predicted signal peptide followed by a bipartite nuclear localization signal (NLS). The idea that AeSSP1256 targets the plant nucleus has been confirmed by its transient expression with or without its signal peptide, both in *Nicotiana benthamiana* leaves and A17 *M. truncatula* roots (Gaulin *et al.*, 2018).

In this study, to gain further insight into the role of AeSSP1256, we have investigated its activity in *M. truncatula*. We found that AeSSP1256 promotes pathogen infection of the A17 partially resistant line and restricts root development. Our microscopic studies and whole-transcriptome approaches in A17 *M. truncatula* roots expressing the effector showed that AeSSP1256 triggers nucleolar stress and downregulates host ribosome-related genes. Using yeast-two hybrid (Y2H), co-immunoprecipitation and FRET–FLIM assays, we identified that AeSSP1256 binds a nucleocytoplasmic DExD-box RNA-Helicase (RH) in *M. truncatula* (MtRH10). This interaction leads to the re-localization of MtRH10 to the perinucleolar space, and it is thus diverted away from its RNA target. Imaging studies using promoter:GUS and MtRH10:GFP constructs reveal the exact expression and localization of MtRH10 in the meristematic cells of the A17 root apex. Silencing of the corresponding gene delays root growth and affects expression of ribosome-related genes, while its overexpression counteracts this phenotype. In contrast to its overexpression, silencing of MtRH10 modifies the outcome of the infection, making the tolerant A17 roots susceptible to *A. euteiches* infection. This study demonstrates that soil-borne oomycete effectors possibly trigger nucleolar stress to promote infection by targeting host RHs, which contribute to root development and defense through the ribosome biogenesis pathway.

Materials and Methods

Plant material, microbial strains, and growth conditions

All experiments were carried out using the partially resistant line *M. truncatula* Jemalong-A17. Seeds were cultured *in vitro* and transformed as described by Boisson-Dernier *et al.* (2001); Djébali *et al.* (2009). *Aphanomyces euteiches* (ATCC 201684) zoospore inoculum was prepared as described by Badreddine *et al.* (2008). Root infection was performed using 10^3 zoospores as described by Ramirez-Garcés *et al.* (2016). *Nicotiana benthamiana* plants were grown under a 16 h : 8 h, 24°C : 20°C, light : dark photoperiod at 70% humidity. *Escherichia coli* (DH5α, DB3.1), *A. tumefaciens* (GV3101::pMP90) and *A. rhizogenes* (ARQUA-1) strains were grown on LB medium using the appropriate antibiotics.

Construction of plasmid vectors and *Agrobacterium*-mediated transformation

The green fluorescent protein (GFP) control plasmid (pK7WGF2), and the *35S:AeSSP1256:YFP, 35S:AeSSP1256:GFP, 35S:SP-AeSSP1256:GFP* (AeSSP1256 sequence with its own signal peptide) and minus or plus signal peptide *35S:AeSSP1256:GFP:KDEL* constructs are described in Gaulin *et al.* (2018). The primers used in this study are listed in Supporting Information Table S1. *Medicago truncatula* candidates sorted by Y2H assay (Table S2) were amplified using Pfx Accuprime polymerase (12344024; Thermo Fisher, Waltham, MA, USA) and introduced into the pENTR/D-TOPO vector by TOPO cloning (K240020; Thermo Fisher) and then transferred into the pK7WGF2, pK7FWG2 (http://gateway.psb.ugent.be/), pAM-PAT-35S::GTW:CFP and pAM-PAT-35S::CFP:GTW binary vectors. The cloning of the *MtRH10* gene (Legoo: MtrunA17_Chr5g0429221) into pK7WGF2 produced the *GFP:MtRH10* construct.

Using pENTR/D-TOPO:AeSSP1256, as described previously (Gaulin *et al.*, 2018), AeSSP1256 was transferred by LR recombination into pAM-PAT-35S::GTW:3HA to create an *AeSSP1256:HA* construct for co-immunoprecipitation and Western blot experiments, and into pUBC-RFP-DEST (Grefen *et al.*, 2010) to obtain the *AeSSP1256:RFP* construct for confocal analyses. For RNAi of MtRH10, a 328 nucleotide sequence in the 3′UTR was amplified by polymerase chain reaction (PCR; Table S1), introduced into the pENTR/D-TOPO vector and LR cloned into the pK7GWiWG2(II)-RedRoot binary vector to obtain the RNAi MtRH10 construct. This vector allows hairpin RNA expression and contains the red fluorescent marker DsRED under the constitutive *Arabidopsis* Ubiquitin10 promoter. For MtRH10 promoter expression analyses, a 1441 nucleotide region downstream of the start codon of the *MtRH10* gene was amplified by PCR (Table S1), fused to the *β-glucuronidase* gene (using the pICH75111 vector (Engler *et al.*, 2014)) and inserted into the pCambia2200:DsRED derivative plasmid (Fliegmann *et al.*, 2013) by Golden Gate cloning to generate the PromoterMtRH10:GUS vector.

Medicago truncatula composite plant hairy roots were generated as described elsewhere (Boisson-Dernier *et al.*, 2001) using the ARQUA-1 *Agrobacterium rhizogenes* strain. *Agrobacterium tumefaciens-transformed* strains were syringe-infiltrated into *N. benthamiana* as described by Gaulin *et al.* (2002).

RNA-Seq experiments

For *35S:GFP* and *35S:SP-AeSSP1256:GFP* RNA-Seq analysis, the total RNA of four biological replicates of transformed roots

were extracted. Before harvest, roots were checked for GFP-fluorescence by live macro-imaging (Axiozoom; Zeiss) and the GFP-positive roots were excised from the plants. Four replicates were prepared for each condition, with one replicate corresponding to the pool of transformed roots excised from 20–40 transgenic plants. Total RNA was extracted using the E.Z.N.A.® total RNA kit (Omega Bio-tek, Norcross, GA, USA) and purified using the Monarch® RNA Cleanup Kit (NEB, Ipswich, MA, USA). cDNA libraries were produced using the MultiScribe™ Reverse Transcriptase kit using a mix of random and poly-T primers under standard conditions for real-time polymerase chain reaction (RT-PCR). Library preparation was performed using the GeT-PlaGe genomic platform (https://get.genotoul.fr/en/) and sequenced using a HiSeq3000 sequencer (Illumina, San Diego, CA, USA). The raw data were trimmed with TrimGalore (v.0.6.5) (https://github.com/FelixKrueger/TrimGalore) with cutadapt and FastQC options, and mapped to *M. truncatula* cv Jemalong A17 reference genome v.5.0 (Pecrix *et al.*, 2018) using Hisat2 (v.2.1.0) (Kim *et al.*, 2019). Samtools (v.1.9) algorithms 'fixmate' and 'markdup' (Li *et al.*, 2009) were used to clean alignments from duplicated sequences. Reads were counted with HTseq (v.0.9.1) (Anders *et al.*, 2015) using the reference GFF file. The count files were normalized and differentially expressed genes (DEGs) were identified using the DESeq2 algorithm (Love *et al.*, 2014); false-positive hits were filtered using a high-throughput sequencing (HTS) filter (Rau *et al.*, 2013). The threshold of the adjusted *P*-values was set to 1×10^{-5} ($P_{adj} < 1 \times 10^{-5}$). Gene ontology (GO) enrichment of DEGs was performed using topGO (Alexa & Rahnenfuhrer, 2020) software. RNA-Seq experiments on susceptible F83005.5 (F83) plants infected by *A. euteiches* are described in Gaulin *et al.* (2018).

RNA extraction and quantitative qRT-PCR

Total RNA was extracted using the E.Z.N.A.® Plant RNA kit (Omega Bio-tek). For reverse transcription, 1 μg of total RNA was used, and reactions were performed with the High-Capacity cDNA Reverse Transcription Kit (Applied Biosystems, Foster City, CA, USA). Quantitative reverse transcription polymerase chain reaction was performed using SYBRGreen (Applied Biosystems) on a QuantStudio 6 (Applied Biosystems) device. The primers used are listed in Table S1.

To estimate the extent of infection by *A. euteiches*, the expression of the α-tubulin coding gene (*Ae_22AL7226* (Gaulin *et al.*, 2008)) was analyzed. The *Histone 3-like* and *EF1α* genes of *M. truncatula* (Rey *et al.*, 2013) were used to normalize *A. euteiches* RNA abundance during infection. For *Aphanomyces* quantification within *AeSSP1256*-expressing roots, five technical replicates and three biological replicates were performed for each time point. A technical replicate is a pool of three to five root systems from distinct composite plants' hairy roots from one *M. truncatula* transformation. Biological replicates correspond to infection assays performed on independent *M. truncatula* transformation assays. Thus, for each time point and construct, 45–75 transformed root systems were analyzed. For *MtRH10* gene quantification, four technical replicates and two biological replicates were performed for each time point (30–40 root systems analyzed per time point). For missense *MtRH10* experiments, cDNA from five samples was used, given that a sample was a pool of five plants ($n = 25$ plants for each construct). For *A. euteiches* quantification in infected roots transformed by GFP:MtRH10, RNAi MtRH10 constructs or in GFP control roots, three technical replicates and two biological replicates were performed each time (*c.* 50 root systems for GFP:MtRH10 or RNAi MtRH10, and 91 for GFP control plants). The relative expression of *Ae* α-tubulin and *MtRH10* helicase genes was calculated using the $2^{-\Delta\Delta C_t}$ method (Livak & Schmittgen, 2001). For reverse transcription polymerase chain reaction (qRT-PCR) validation of RNA-Seq experiments, cDNA were derived from five technical replicates, and two biological replicates. The relative expression levels of 17 ribosome-related genes (Table S3) were calculated using the $2^{-\Delta\Delta C_t}$ method.

Yeast two-hybrid assays

An ULTImate Y2H™ assay was carried out by Hybrigenics Services (https://www.hybrigenics-services.com) using the mature form of AeSSP1256 (20–208 aa) as bait against a library prepared from *M. truncatula* roots infected by *A. euteiches*. The library was prepared by Hybrigenics Services using a mixture of RNA isolated from uninfected *M. truncatula* F83005.5 (±12%), *M. truncatula* infected with *A. euteiches* ATCC201684 harvested 1 d post-infection (±46%), and *M. truncatula* infected with *A. euteiches* harvested 6 d post-infection (±42%). This library is now available to other customers at Hybrigenics Services. For each interaction identified during the screen performed by Hybrigenics (65 million interactions tested), a 'Predicted Biological Score (PBS)' was given, which indicates the reliability of the identified interaction. The PBSs range from 'A' (very high confidence of interaction) to 'F' (experimentally proven technical artifacts). In this study, we kept candidates with PBS values from 'A' to 'C' for validation.

Analysis of the amino acid sequence of *MtRH10*

MtRH10 (*MtrunA17_Chr5g0429221*) putative nuclear localization signal (NLS) motifs were predicted by cNLS Mapper with a cut-off score of 4.0 (Kosugi *et al.*, 2009). The putative nuclear export signal (NES) motifs were predicted using NES Finder v.0.2 (http://research.nki.nl/fornerodlab/NES-Finder.htm) and the NetNES 1.1 Server (la Cour *et al.*, 2004). Conserved motifs and domains of DExD-box R were found using the ScanProsite tool on the ExPASy website (https://prosite.expasy.org/scanprosite/).

For the phylogenetic tree, 29 sequences were selected based on BlastP results (cut off *e*-value $< 10^{-30}$) using *MtRH10* on the *Medicago truncatula* genome portal (Mt5.0 version, https://medicago.toulouse.inra.fr/). Three sequences with an alignment length < 30% (MtrunA17_Chr1g0155691; MtrunA17_Chr8g0349951; MtrunA17_Chr1g0155211) were removed from the dataset. The phylogenetic tree was constructed and visualized using the CLC Workbench (Qiagen), with ClustalW alignment and the neighbor-joining (NJ) method with default parameters and a bootstrap value of 1000.

Immunoblot analysis

For *N. benthamiana* protein analyses, at least three independent agroinfiltration assays were performed for each construct. Each assay represents the infiltration of three plants on two distinct leaves per plant. A technical replicate is a pool of the two leaves from the same plant (three technical replicates per assay). Each blot was performed with technical replicates from one assay, and blots were repeated using the replicates from the independent assays. For *M. truncatula* protein analyses, each blot was repeated using proteins extracted from the different biological replicates. Immunoblots were performed as described in Ramirez-Garcés *et al.* (2016) using 30 μg of total protein separated on 10% Stain-Free SDS-PAGE gels (1610173; Bio-Rad). For GFP detection, an anti-GFP from mouse IgG1κ (clones 7.1 and 13.1; 11814460 001, Roche) was used. A monoclonal anti-hemagglutinin (HA) antibody produced in mouse (H9658, Sigma-Aldrich) was used for HA detection. An anti-mouse secondary antibody coupled to horseradish peroxidase (BioRad; 170-6516) was used with an ECL Clarity Kit (BioRad; 170-5060) for visualization.

Co-immunoprecipitation assay

Co-immunoprecipitation was performed using *N. benthamiana* infiltrated leaves. Biological and technical replicates were harvested 24 h after treatment, and total proteins (50 μg) were incubated for 3 h at 4°C with 30 μl of GFP-Trap Agarose beads (gta-20; Chromotek, Planegg, Germany). After the washing steps, the GFP-beads were boiled in SDS loading buffer (Merck; S3401) and immunoblotting was performed.

Confocal microscopy

Scanning was performed on a TCS SP8 confocal microscope (Leica, Microsystems, UK). For GFP and GFP variant recombinant proteins, the excitation wavelength was 488 nm, with emission absorbance between 500 nm and 550 nm, whereas an excitation wavelength of 543 nm was used for RFP variant proteins, with emission absorbance between 560 nm and 600 nm. Images were acquired with a ×40 or ×20 water immersion lens and correspond to Z projections of the scanned tissues (*c.* 5 μm depth). All confocal images were analyzed and processed using the ImageJ software package (http://rsb.info.nih.gov/ij/).

Cytological observations of transformed roots

Roots of composite plants were prepared as described previously (Ramirez-Garcés *et al.*, 2016). For each construct, a total of nine roots from three independent transformation experiments were used. NDPview2 software was used to observe longitudinal root sections of GFP or missense MtRH10 plants and to measure the root apical meristem (RAM) was used for all other measurements. Average RAM cell sizes were estimated by measuring all the cells from the same layer from the quiescent center to the RAM boundary. Mean values were then calculated from > 200 cells. In the elongation zone (EDZ) of GFP, AeSSP1256: GFP or missense *MtRH10* roots, cell area and cell perimeter were measured in a rectangular measuring *c.* 300 × 600 μm (two selections per root). To obtain a normalized cell perimeter, each cell perimeter was proportionally recalculated for a 500 μm^2 area standard cell. To estimate cell shape differences, considering that cortical cells in the EDZ of GFP control roots are mostly rectangular, we measured the perimeter bounding rectangle (PBR), which represents the smallest rectangle enclosing the cell. We then calculated the perimeter : PBR ratio. Rectangular cells have a perimeter : PBR ratio close to 1.

Measurement of nucleolar surface

Ten roots from two independent *M. truncatula* transformations were fixed for 2 h under vacuum in fixation buffer 4% paraformaldehyde (15710; Electron Microscopy Sciences), 50 mM sodium cacodylate (12300; Electron Microscopy Sciences), 0.1% Triton X-100 (T8787; Merck) diluted in TBS 1× (ET220; Euromedex, Souffelweyersheim, France) and incubated overnight at 4°C. After washing in TBS 1×, roots were stained with 4′,6-diamidino-2-phenylindole (DAPI; D8417; Merck) for 30 min under vacuum before confocal imaging using the GFP channel (excitation 488 nm; emission 500–550 nm), DAPI channel (excitation 405 nm; emission 415–450 nm) or bright field (BF). The nucleolar surface was estimated using ImageJ software by combining measurements based on the three channels (GFP, DAPI, BF).

Fluorescent resonance energy transfer (FRET)/fluorescence lifetime imaging microscopy (FLIM) measurements

For protein–protein interactions, *N. benthamiana* agroinfiltrated leaves were analyzed as described previously (Tasset *et al.*, 2010). For protein–nucleic acid interactions, samples were prepared as described in (Camborde *et al.*, 2017; Escouboué *et al.*, 2019). Nucleic acid staining was performed by vacuum infiltrating a 5 μM Sytox Orange (S11368; Thermo Fisher) solution. Samples were observed on an inverted microscope (Eclipse TE2000E; Nikon, Tokyo, Japan). For RNase treatment, foliar discs were incubated for 15 min at room temperature with 0.5 mg ml^{-1} RNase A (R6513; Merck) before nucleic acid staining. Fluorescence lifetime measurements were performed in the time domain using a streak camera as described by Camborde *et al.* (2017). The fluorescence lifetime of the donor (GFP) was experimentally measured in the presence and absence of the acceptor (Sytox Orange). FRET efficiencies (E) were calculated by comparing the lifetime of the donor in the presence of the acceptor (τ_{DA}) to that in the absence of the acceptor (τ_D): $E = 1 - (\tau_{DA})/(\tau_D)$. Statistical comparisons between control (donor) and assay (donor + acceptor) lifetime values were made using Student's t-test. For each experiment, nine leaf discs collected from three agroinfiltrated leaves were used, and at least two independent infiltration assays were performed. A minimum of 30 nuclei were scanned to ensure the statistical significance of the data.

Results

AeSSP1256 impairs *Medicago truncatula* root development and promotes pathogen infection

To investigate the function of AeSSP1256 in the host plant, we expressed the *AeSSP1256* gene in *M. truncatula* A17-Jemalong roots (*35S:SP-AeSSP1256:GFP*). In these 'composite' plants generated using *Agrobacterium rhizogenes,* only the root system is transformed (Boisson-Dernier *et al.*, 2001). The presence of AeSSP1256 in the plant strongly affects root development, as shown in the photographs in Fig. 1(a). The total number of roots and primary root length per plant are significantly lower in AeSSP1256-expressing roots than in GFP control roots (Fig. 1b). The presence of the GFP-tagged AeSSP1256 protein (expected size 46.5 kDa) was confirmed by Western-blot analysis using anti-GFP antibodies on total proteins extracted from the transformed *Medicago truncatula* roots (Fig. 1c). A slight cleavage of the AeSSP1256-fusion protein was observed thanks to the presence of a GFP-band at *c.* 26 kDa. To check if the observed aberrant root development is due to the GFP-tag, we confirmed the phenotype on A17 roots expressing a HA-tagged version of AeSSP1256 (Fig. 1c,d).

To evaluate whether AeSSP1256 modifies the outcome of the infection, AeSSP1256:GFP-expressing roots were inoculated with *A. euteiches* zoospores. We observed browning of the roots, indicating root rot symptoms due to *A. euteiches*, from 7 to 21 d after inoculation of the pathogen in both the control GFP-roots and in AeSSP1256-expressing roots, but with greater severity in roots expressing the effector (Fig. 1e). We carried out RT-qPCR analyses at 7-, 14- and 21 d post-inoculation to monitor pathogen development and compared them with infected GFP-control roots. Our results showed that the presence of the effector rendered the partially resistant A17 *Medicago* roots more susceptible to the pathogen (1.5–5 times higher accumulation of the pathogen with time) (Fig. 1f). Thus, expression of AeSSP1256 alters root development and enhances host root infection.

AeSSP1256 localizes to the nucleolus rim and triggers nucleoli enlargement in *M. truncatula* root cells

The *Medicago* composite plant hairy roots were used to confirm the subcellular localization of the effector in the host. As depicted in Fig. 2(a), confocal analyses showed a fluorescent circle around the nucleolus for AeSSP1256 GFP-fusion protein in *Medicago* hairy roots cells. The nucleolus rim is not observed in GFP-transformed hairy roots (*35S:GFP)*. We next found evidence that supports the subcellular localization of AeSSP1256 through confocal imaging of *N. benthamiana* leaves agroinfiltrated with *35S:SP-AeSSP1256:RFP* in combination with *35S:GFP:H2B* (Histone 2B). An RFP-fluorescence pattern at the nucleolus rim which surrounds the nucleolar GFP fluorescence pattern of GFP:H2B proteins was detected (Fig. S1), thus demonstrating the presence of AeSSP1256 at the nucleolus rim *in planta*.

We noticed that the peri-nucleolus localization of AeSSP1256 in *Medicago* roots seems to be correlated with enlarged nucleoli, as revealed in DAPI-stained samples (Fig. 2b). Measurements of nucleoli size from image analysis confirmed a variation from 4.5 μm^2 ($\pm$1.9) for control roots to 6.6 μm^2 ($\pm$3) for AeSSP1256:GFP-expressing roots (Fig. 2c). Changes in morphology and nucleolus size are linked to nucleolar activity (Ohbayashi & Sugiyama, 2018). Perturbation of the nucleolar structure ultimately impairs ribosome biogenesis and triggers so-called nucleolar/ribosomal stress (Ohbayashi & Sugiyama, 2018). Thus, the enlargement of *Medicago* nucleoli in the presence of AeSSP1256 suggests that the effector induces nucleolar stress by interfering with the ribosome biogenesis pathway.

To find out whether the effect of AeSSP1256 on *Medicago* roots is linked to the peri-nucleolar localization of the effector, a KDEL-endoplasmic reticulum (ER) retention signal was added to the *35S:SP-AeSSP1256:GFP* construct (Fig. S2a). The observed GFP fluorescence pattern in these transgenic roots is similar to that detected in roots transformed with the mCherry-ER marker (*ER-rb-CD3-960* construct) (Fig. S2a,b). As expected, this points to the retention of the effector in the endoplasmic reticulum. By contrast, a nuclear fluorescence pattern is detected when *Medicago* roots are transformed with a *35S:AeSSP1256:GFP:KDEL* construct (Fig. S2a,b). In each of these situations, the fluorescence pattern is distinctly different from that detected in GFP control roots. The presence of the different versions of the effector in transgenic roots was investigated using Western-blot analysis (Fig. S2c). As illustrated in Fig. S2(d) and quantified in Fig. S2(e), abnormal root development was observed only when the AeSSP1256 effector accumulated in the nuclei of *Medicago*. Taken together, our results demonstrate that the localization of the effector to the nucleolus rim is important for its biological activity.

AeSSP1256 affects the expression of genes related to ribosome biogenesis

We performed comparative whole-genome transcriptomic analysis using paired-end sequencing of four biological replicates of *35S:GFP* and *35S:SP-AeSSP1256:GFP* transformed roots. In all, we identified 4391 DEGs, 2129 of which were upregulated and 2262 of which were downregulated (adjusted *P*-value $< 1 \times 10^{-5}$; Table S3a). To identify the function of the DEGs, we performed gene set enrichment analysis using the TopGO software package for the three main GO categories (Fig. 3a; Table S3b): biological process, cellular component, and molecular function. The upregulated DEGs corresponded mainly to the 'photosynthesis' GO term. In the downregulated DEGs, we identified 'ribosome biogenesis', 'organonitrogen compound biosynthesis' and 'cellular amide metabolic processes' GO terms to be among the most represented, all of which were strikingly downregulated. We next selected 17 *M. truncatula* genes for qRT-PCR analysis to confirm the effect of AeSSP1256 on the ribosome biogenesis pathway of the host. First, we chose ten Arabidopsis genes that control plant development (i.e. mutants with shorter root phenotypes) (Table S3c) by Blast searches (> 80% identity) in the A17 line r5.0 genome portal (Pecrix *et al.*, 2018). We also selected seven genes coding for ribosomal

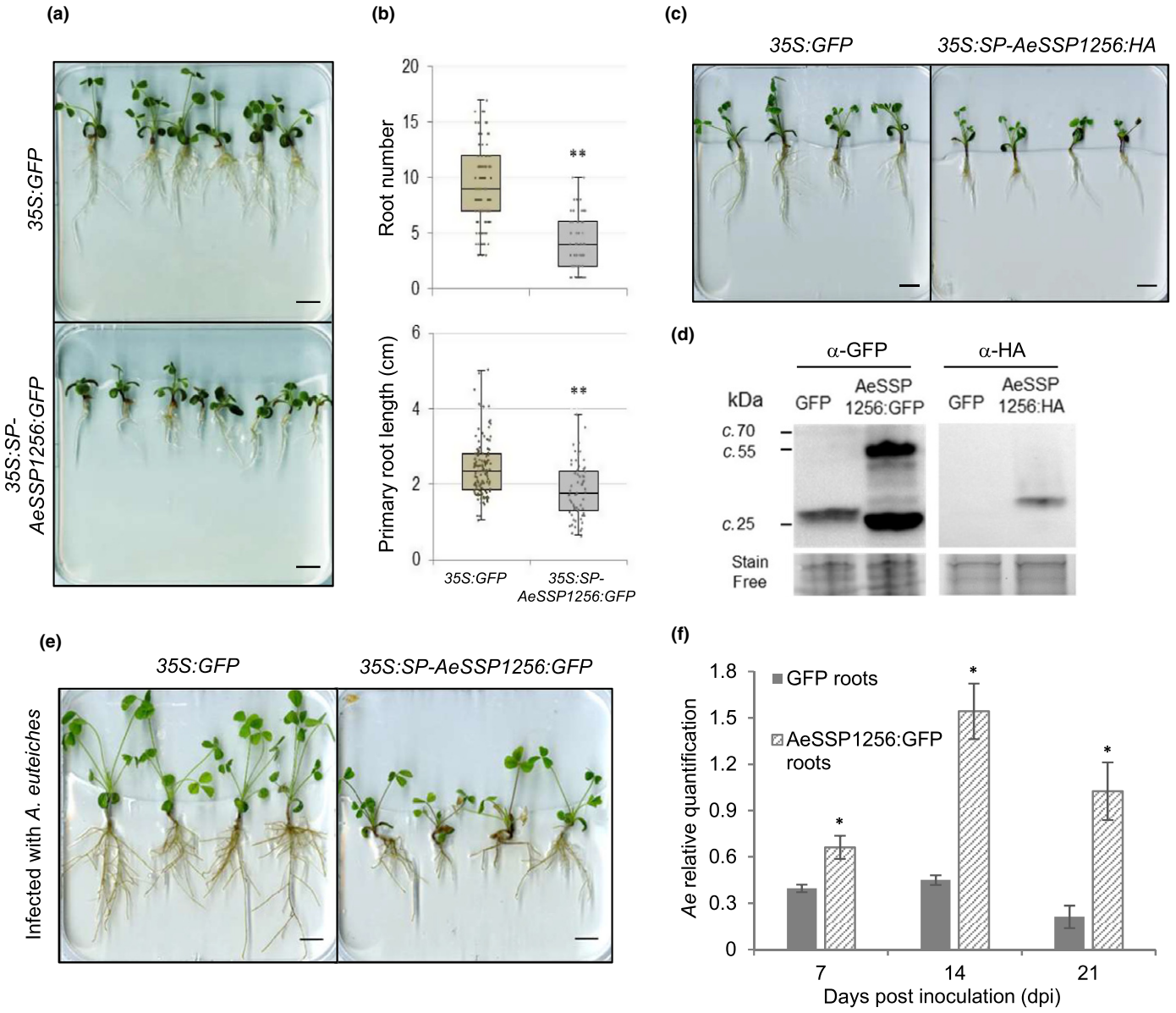

Fig. 1 AeSSP1256 perturbs *Medicago truncatula* root development and increases its susceptibility to *Aphanomyces euteiches*. Plants of the tolerant *M. truncatula* A17 line were transformed using *Agrobacterium rhizogenes* with *35S:GFP* or *35S:SP-AeSSP1256:GFP* constructs to generate composite plants in which only the root system was transformed. (a) Representative 35S:GFP and 35S:SP-AeSSP1256:GFP *M. truncatula* plants grown over 21 d. Note the reduced growth of the roots expressing AeSSP1256:GFP compared those expressing free green fluorescent protein (GFP). Bar, 1 cm. (b) Quantification of root number (upper panel) and primary root length (in cm; bottom panel) of transformed roots of control and 35S:SP-AeSSP1256:GFP plants at 21 d after transformation (DAT). Results were obtained from five independent experiments for a total of 126 GFP-transformed plants and 79 AeSSP1256:GFP-transformed plants. The boxes indicate the interquartile range (25th to the 75th percentile). The central line within the boxes represents the mean value. The whiskers indicate the minimum and maximum values. The jittered data points were superimposed onto the box plot to show the underlying distribution of the data. The asterisks indicate significant differences (Student's *t*-test; **, $P < 0.001$). (c) Representative *M. truncatula* roots transformed with the *35S:GFP* or *35S:SP-AeSSP1256:HA* constructs at 21 DAT. Note the reduction in the development of the root system. Bar, 1 cm. (d) Western-blot analysis using total proteins extracted from transformed *M. truncatula* roots at 21 DAT and anti-GFP or anti-HA antibodies. Protein loading was verified by stain-free imaging of polyacrylamide gel. The representative blot (from three independent analyses) shows a band at *c.* 28 kDa for the free GFP expressed from a pK7WGF2 vector in control roots. The GFP-tagged effector expressed from the pK7FWG2 vector is probably cleaved, with an expected band at *c.* 46.5 kDa and an additional band for the free GFP. (e) Representative root rot disease symptoms observed in 35S:GFP and 35S:SP-AeSSP1256:GFP *M. truncatula* plants at 14 d post-inoculation with *A. euteiches*. Transformed-roots (21 DAT) were inoculated with 10 µl of *A. euteiches* zoospores (10^5 spores ml^{-1}). Bar, 1 cm. (f) Relative quantification of the *A. euteiches* tubulin gene in transformed roots treated by the pathogen, as analyzed by quantitative polymerase chain reaction (qPCR). 35S:GFP- and 35S:SP-AeSSP1256:GFP-transformed roots were inoculated with 10 µl of *A. euteiches* zoospores (10^5 spores ml^{-1}). Data were collected from three to five different pools of roots for a total of 45 to 75 plants per time point at 7, 14 and 21 d post-infection. Bars represent the mean values (±SE). Asterisks indicate significant differences (Student's *t*-test; *, $P < 0.05$).

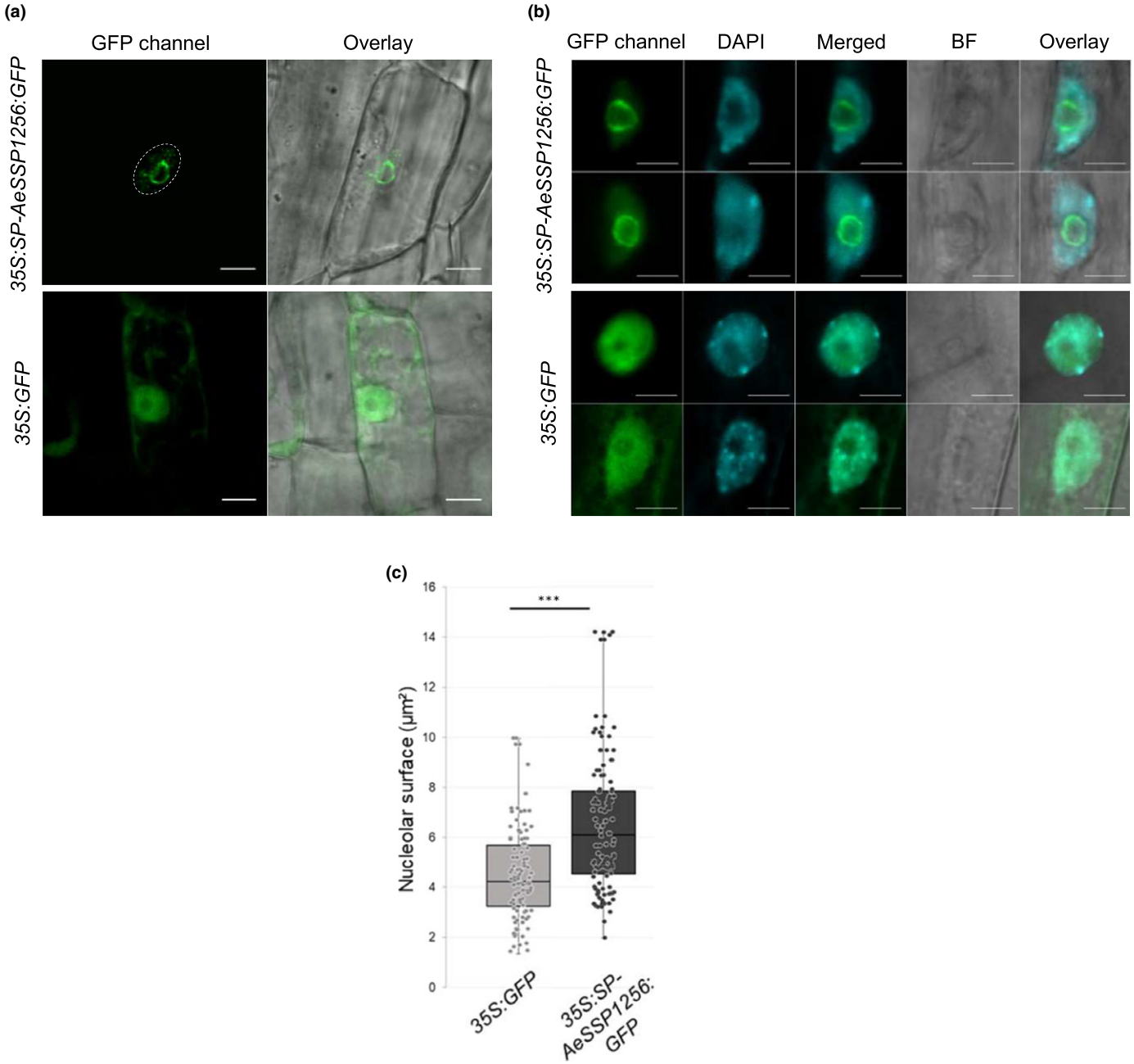

Fig. 2 AeSSP1256 localizes to the nucleolus rim and triggers nucleoli size enlargement in *Medicago truncatula* roots. Hairy root transformation of *M. truncatula* A17 line, using *Agrobacterium rhizogenes* to generate composite plants where only the root system was transformed. (a) Representative confocal analysis images of *M. truncatula* roots 21 d after *Agrobacterium* transformation (DAT) with *35S:GFP* or *35S:SP-AeSSP1256:GFP* constructs. Note that the free green fluorescent protein (GFP) shows a nucleocytoplasmic localisation, while AeSSP1256:GFP is localized as a ring around the nucleolus. Dashed lines indicate the nucleus. Bar, 5 µm. (b) Roots were fixed and nuclei were stained with 4′,6-diamidino-2-phenylindole (DAPI). Note the enlargement in the nucleoli surface where AeSSP1256:GFP proteins are present, as compared to cells expressing free GFP. BF, bright field. Bar, 5 µm. (c) Nucleoli surface measurements (in μm^2) for root cells expressing *35S:GFP* or *35S:SP-AeSSP1256:GFP* at 21 DAT. The boxes indicate interquartile range (25^{th} to the 75^{th} percentile). The central line within the boxes represents the mean value. The whiskers indicate the minimum and maximum values. The jittered data points were superimposed onto the box plot to show the underlying distribution of the data $n = 108$ nuclei for GFP, and 124 nuclei for AeSSP1256:GFP, using a total of 10 different roots for each construct. Independent experiments were conducted for a total of 126 GFP-transformed plants and 79 AeSSP1256:GFP-transformed plants. Asterisks indicate significant differences (Student's *t*-test; ***, $P = 1.51 \times 10^{-9}$).

proteins and related to 'ribosome biogenesis' in *M. truncatula* for expression analysis based on the KEGG pathway map (https://www.genome.jp/kegg-bin/show_pathway?ko03008) (Table S3c). As shown in Fig. 3(b), all of the seventeen selected genes from *M. truncatula* are downregulated in the presence of AeSSP1256. At this point, our results pointed to a perturbation of the ribosome biogenesis pathway of the host plant by the AeSSP1256 effector.

(a)

	Rank	GO ID	GO name	Total	Significant (%)	Expected	*P*-value
4391 DEGs							
Downregulated	1	GO:1901566	Organonitrogen compound biosynthetic process	1328	254 (19%)	101	< 1e−30
2262 total	2	GO:0006518	Peptide metabolic process	737	169 (23%)	56.05	< 1e−30
	3	GO:0043603	Cellular amide metabolic process	865	185 (21%)	65.78	< 1e−30
	4	GO:0042254	Ribosome biogenesis	573	144 (25%)	43.58	< 1e−30
	5	GO:0043604	Amide biosynthetic process	761	169 (22%)	57.87	< 1e−30
Upregulated	1	GO:0015979	Photosynthesis	186	51 (27%)	9.21	1.70E−24
2129 total	2	GO:0009765	Photosynthesis, light harvesting	24	15 (62%)	1.19	2.00E−14
	3	GO:0019684	Photosynthesis, light reaction	94	23 (24%)	4.65	1.20E−10
	4	GO:0007154	Cell communication	745	68 (9%)	36.87	6.90E−07
	5	GO:0007165	Signal transduction	610	58 (9%)	30.19	1.30E−06

(b)

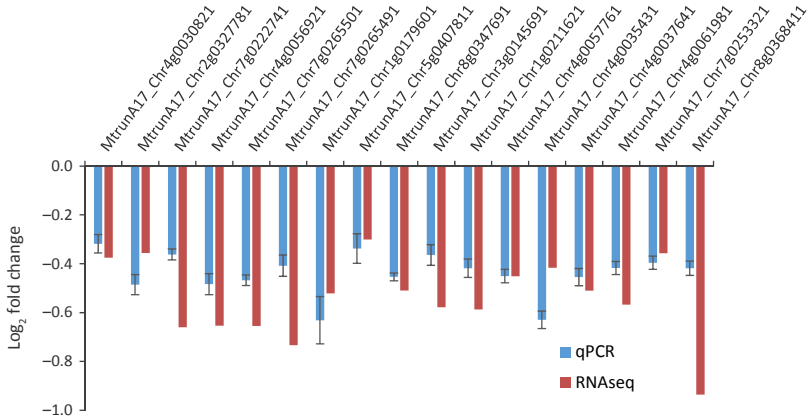

(c)

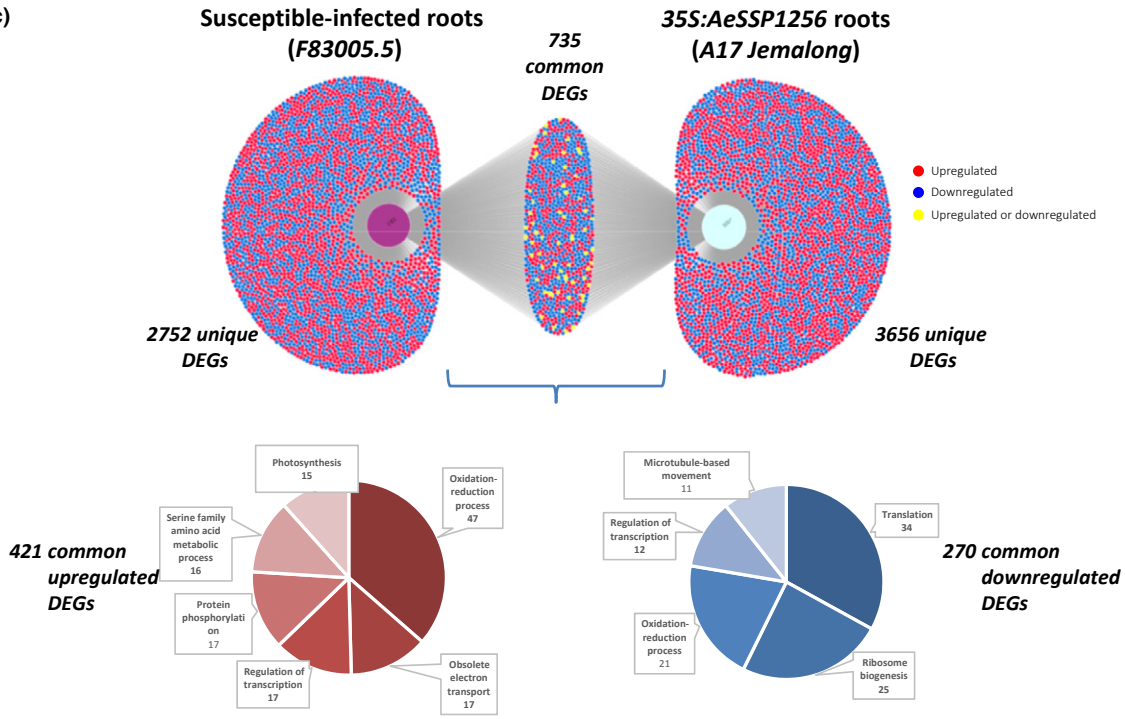

Fig. 3 Transcriptomic analyses reveal downregulation of genes related to ribosome biogenesis in both AeSSP1256-expressing roots and *Aphanomyces euteiches-infected* roots. (a) Top five enriched gene ontology (GO)-terms of downregulated and upregulated genes, obtained using classical gene set enrichment analysis (GSEA) with Fischer's exact test. Expected, enrichment threshold; Significant, number of differentially expressed genes (DEGs); Total, number of genes of the category in the genome. (b) Comparison of RNA-Seq ($n = 4$) and quantitative reverse transcription polymerase chain reaction (qRT-PCR) ($n = 5$, different samples of the RNA-Seq) analysis of selected ribosome biogenesis-related genes in AeSSP1256-expressing roots. Bars represent the mean values (±SE). (c) Upper panel: Venn diagram of DEGs for two RNA-Seq experiments (number of genes) in susceptible *Medicago truncatula* F83005.5 roots infected with *A. euteiches* at 9 dpi (data from Gaulin *et al*., 2018) and the tolerant *M. truncatula* A17 line expressing the AeSSP1256:GFP effector (this study). Bottom panel: DEGs that are specific or common to the F83-infected line and the AeSSP1256-expressing roots (downregulated (blue) and upregulated (red)). Lower panel: Pie charts depicting the number of common DEGs associated with a GO term. Only GO terms associated with > 10 genes are represented. GO terms related to 'translation and ribosome-biogenesis' are the most represented in the downregulated category.

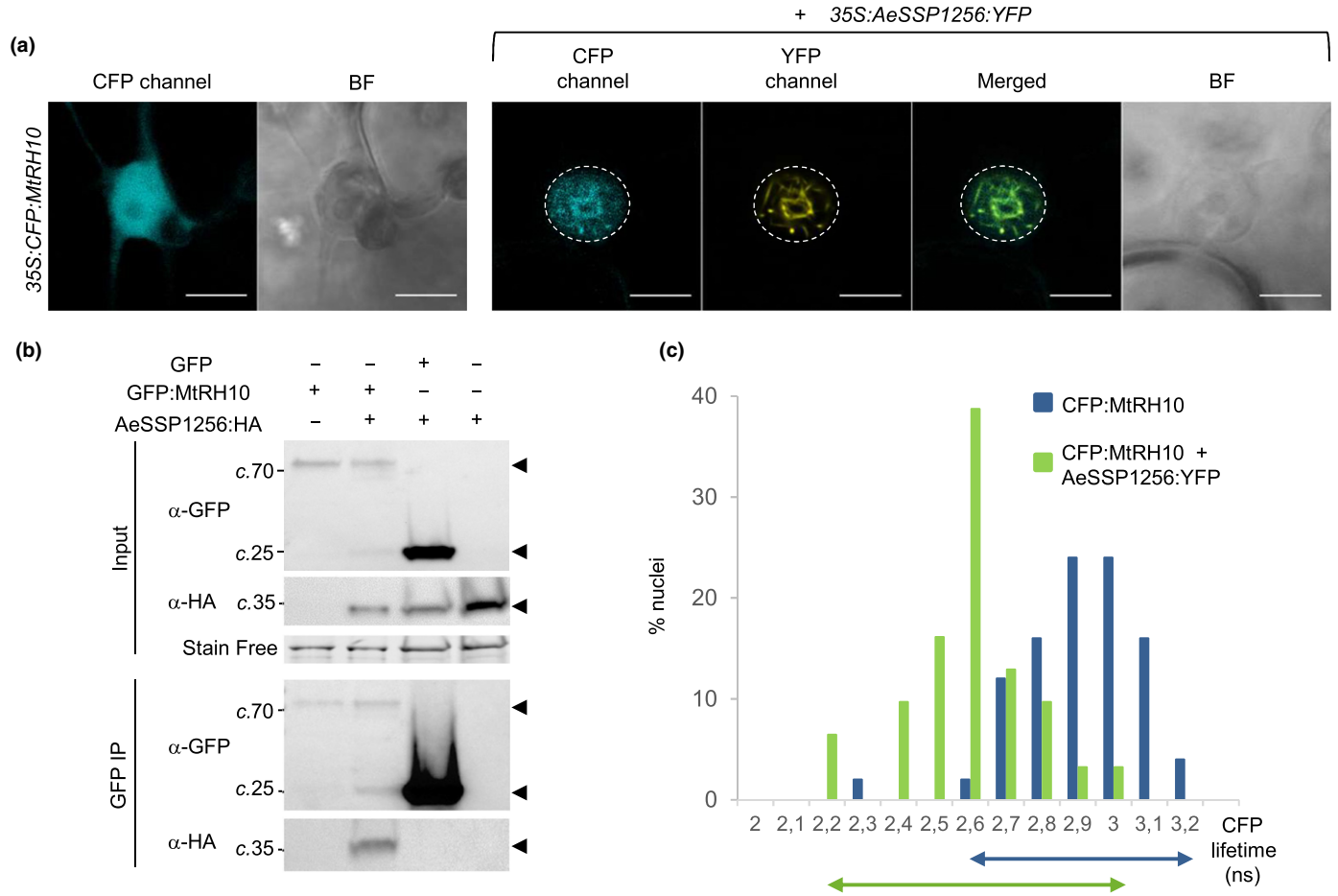

Fig. 4 AeSSP1256 associates with and relocalizes a nucleocytoplasmic host RNA helicase (MtRH10) to the nucleolus rim in *Nicotiana benthamiana* cells. Four-week-old *N. benthamiana* leaves were inoculated or co-inoculated with *Agrobacterium tumefaciens* harbouring the *35S:AeSSP1256:YFP* or *35S:CFP:MtRH10* constructs. For each construct, three independent replicates were performed; per repetition, two leaves from two distinct leaf stages and three independent plants were agroinfiltrated. (a) Representative fluorescence images obtained using confocal laser scanning microscopy 1 d after transient expression in leaves. Samples were randomly selected for fluorescence detection. MtRH10 shows a nucleocytoplasmic localization (left panel), while the presence of AeSSP1256 re-localizes MtRH10 to the peri-nucleolar space around the nucleolus (right panel) where the effector is localized. BF, bright field. The white dashed lines indicate the nuclear membrane. Bar, 10 μm. (b) Representative immunoprecipitation (IP) of protein extracts from agroinfiltrated leaves using GFP-Trap beads, confirming that AeSSP1256 associates with MtRH10. Expression of constructs in the leaves is indicated by 'plus' symbols (+). Protein size markers are indicated in kDa and protein loading is verified by stain-free imaging of polyacrylamide gel. Protein fusion bands are indicated by arrows. Upper panel: anti-GFP and anti-HA blots to confirm the presence of fusion proteins in the input fractions. Lower panel: anti-GFP and anti-HA blots on output fractions to reveal the presence of the corresponding protein. (c) Cyan fluorescent protein (CFP) lifetime distribution of the *35S:CFP:MtRH10* construct when expressed alone or in combination with the *35S:AeSSP1256:YFP* construct in transiently transformed *N. benthamiana* leaves. Histograms show the distribution of nuclei (%) according to classes of CFP:MtRH10 lifetime in the absence (blue bars) or presence (green bars) of AeSSP1256:YFP. The arrows represent the CFP lifetime distribution range. Statistical analyses are provided in Table 2. The significant decrease in fluorescence lifetime indicates a close association between AeSSP1256 and MtRH10.

We next investigated if the effector by itself mimics responses observed during pathogen infection of *M. truncatula*. This was done by mining the RNA-Seq experiment that we previously developed on the susceptible F83005.5 (F83) *M. truncatula* line (Gaulin *et al.*, 2018). As shown in the Venn diagram depicting both specific and common upregulated and downregulated genes in AeSSP1256:GFP-expressing roots and in susceptible F83-infected roots 9 d after infection, 735 are common DEGs (Fig. 3c; Table S3d). A number of the common upregulated DEGs are associated with 'oxido-reduction and photosynthesis' GO terms, while the downregulated DEGs are associated with 'ribosome biogenesis' and 'translation' GO terms. With regard to the total DEG analysis, these two categories mostly consist of downregulated genes, which occupy, respectively, 92% and 84% of the common DEGs (Fig. 3c; Table S3d,e). These results show that expression of AeSSP1256 within the host root cells mimics some of the effects induced by the pathogen when it infected the susceptible *Medicago* line.

AeSSP1256 associates with a nucleocytoplasmic host RNA helicase (MtRH10) and relocalizes it to the nucleolus rim

A yeast two hybrid (Y2H) library composed of cDNA from *M. truncatula* roots infected with *A. euteiches* was screened with the effector to identify AeSSP1256 protein targets. Through screening, we identified eight *M. truncatula* coding genes, seven

Table 1 Fluorescent resonance energy transfer–fluorescence lifetime imaging microscopy (FRET–FLIM) measurements of a *Medicago truncatula* cyan fluorescent protein (CFP)-tagged RNA helicase (MtRH10) in the presence or absence of the AeSSP1256:YFP effector, to detect protein–protein interactions.

Donor	Acceptor	τ[a]	SEM[b]	*n*[c]	*E*[d]	*P*-value[e]
CFP:MtRH10	–	2.86	0.023	50	–	–
CFP:MtRH10	AeSSP1256:YFP	2.53	0.031	31	11.1	2.56×10^{-12}

[a]Mean lifetime in nanoseconds (ns).
[b]Standard error of the mean.
[c]Total number of measured nuclei.
[d]FRET efficiency in %: $E = 1 - (\tau DA/\tau D)$, where τDA is the lifetime of the donor in the presence of the acceptor, and τD is the lifetime of the donor in the absence of the acceptor.
[e]*P*-value (Student's *t*-test) for the difference between the donor lifetimes in the presence or absence of the acceptor.

Table 2 Fluorescent resonance energy transfer–fluorescence lifetime imaging microscopy (FRET–FLIM) measurements for GFP:MtRH10 with or without Sytox Orange, to detect protein–nucleic acid interactions.

Donor	Acceptor	τ[a]	SEM[b]	*n*[c]	*E*[d]	*P*-value[e]
GFP:H2B	–	2.45	0.025	30	–	–
	Sytox	1.89	0.072	30	23	2.88×10^{-9}
GFP:H2B *(+RNase)*	–	2.36	0.032	32	–	–
	Sytox	1.92	0.056	31	19	1.12×10^{-9}
GFP	–	2.29	0.034	35	–	–
	Sytox	2.30	0.037	36	0	0.94
GFP:MtRH10	–	2.32	0.020	60	–	–
	Sytox	2.08	0.027	60	10.3	1.30×10^{-10}
GFP:MtRH10 *(+RNaSe)*	–	1.94	0.028	46	–	–
	Sytox	1.95	0.035	39	0	0.83

[a]Mean lifetime in nanoseconds (ns).
[b]Standard error of the mean.
[c]Total number of measured nuclei.
[d]FRET efficiency in %: $E = 1 - (\tau DA/\tau D)$, where τDA is the lifetime of the donor in the presence of the acceptor, and τD is the lifetime of the donor in the absence of the acceptor.
[e]*P*-value (Student's *t*-test) for the difference between the donor lifetimes in the presence or absence of the acceptor.

Table 3 Fluorescent resonance energy transfer–fluorescence lifetime imaging microscopy (FRET–FLIM) measurements for GFP:MtRH10 with or without Sytox Orange, in the presence of AeSSP1256:HA, to detect protein–nucleic acid interactions.

Donor + AeSSP1256:HA	Acceptor	τ[a]	SEM[b]	*n*[c]	*E*[d]	*P*-value[e]
GFP:MtRH10 (Relocalized)	–	2.30	0.023	60	–	–
GFP:MtRH10 (Relocalized)	Sytox	2.30	0.020	60	0	0.789

[a]Mean lifetime in nanoseconds (ns).
[b]Standard error of the mean.
[c]Total number of measured nuclei.
[d]FRET efficiency in %: $E = 1 - (\tau DA/\tau D)$, where τDA is the lifetime of the donor in the presence of the acceptor, and τD is the lifetime of the donor in the absence of the acceptor.
[e]*P*-value (Student's *t*-test) for the difference between the donor lifetimes in the presence or absence of acceptor.

of which corresponded to putative nuclear proteins (Table S2). After testing six candidates for co-localization by transient expression in *N. benthamiana* (Fig. S3) we focused on a DExD-box ATP-dependent RH encoded by the *MtrunA17_Chr5g0429221* gene (Mt5.0 version). Indeed, co-expression in *Nicotiana* leaves of the nucleocytoplasmic GFP-RH with a CFP-tagged AeSSP1256 triggered a redistribution of the RH to the perinucleolar space (Fig. 4a). The redistribution of the RH to the nucleolus rim in *N. benthamiana* cells was also confirmed using a HA-tagged version of the effector and Western-blot analysis (Fig. S4a,b).

BLAST analysis revealed that the closest plant orthologs of the RH are AtRH10 in *Arabidopsis thaliana* (UniProtKb: Q8GY84) and OsRH10 in *Oryza sativa* (UniProtKb: A2XKG2) (% similarity 51.2% and 49.2% at the amino acid level), while there is no close ortholog in *N. benthamiana*. These two nucleolar RHs are involved in ribosome biogenesis (Matsumura *et al.*, 2016; Liu & Imai, 2018) and rRNA homeostasis, respectively (Wang *et al.*, 2016). Accordingly, the target *Medicago* protein of AeSSP1256 was named MtRH10. MtRH10 is related to the human nucleolar RH DDX47 (UniProtKb: Q9H0S4) (Sekiguchi *et al.*, 2006) and the yeast nuclear RH RRP3 (UniProtKb: P38712) (O'Day, 1996). MtRH10 harbors predicted putative NESs (positions 7–37; 87–103; 261–271), an NLS (position 384–416) and conserved functional domains, as inferred from its sequence alignment with DDX47, RRP3, AtRH10 and OsRH10 proteins (Fig. S5a).

BLASTP analysis of the *M. truncatula* proteome (https://medicago.toulouse.inra.fr/) revealed that MtRH10 has the highest identity at the amino acid level with MtrunA17_Chr6g0483491 and MtrunA17_Chr7g0236841 (> 62%) and *c.* 53% amino acid identity with MtrunA17_Chr1g0155201. The phylogenetic tree using full amino acid sequences from *M. truncatula* (cut off *e*-value < 10^{-30}) showed that the four sequences are classified within the same group, subdivided into two distinct classes and related to the RH10 family from different species (Fig. S5b). The other *M. truncatula* sequences are less similar and are related to other known DExD-box proteins such as AtRH36 from *Arabidopsis*.

Interaction between AeSSP1256 and MtRH10 was assessed using co-immunoprecipitation and FRET-FLIM experiments. Following immunoprecipitation with GFP beads at 24 dpi, we searched for the presence of the corresponding proteins by Western-blotting. The AeSSP1256:HA proteins were detected in the GFP:MtRH10 immunoprecipitated fraction but not with free GFP (Fig. 4b). We performed a FRET-FLIM analysis on *N. benthamiana* leaves to detect protein–protein interactions. At 24 hpi, we found that the fluorescence lifetime of CFP-MtRH10 was shifted to lower values in the presence of the effector (Fig. 4c). As listed in Table 1, the change in the mean CFP lifetime within the CFP:MtRH10-expressing nuclei from 2.86 ns (in the absence of the effector) to 2.53 ns (in the presence of the YFP-tagged effector) reveals association *in planta*. These data indicate

that the effector interacts with MtRH10 *in vivo* and causes its redistribution to the nucleoli rim.

MtRH10 binding to RNA is disrupted by AeSSP1256

To test whether MtRH10 is functionally active for RNA binding, we examined its interaction with nucleic acids by FRET-FLIM (Förster, 1948; Camborde *et al.*, 2017). The donors were GFP:MtRH10, GFP:H2B or GFP transiently expressed in *N. benthamiana* leaves. Agroinfiltrated samples were collected 1 d after treatment and labelled with Sytox Orange to convert nucleic acids to FRET acceptors. In the absence of Sytox Orange the mean lifetime of GFP:H2B was 2.45 ns, and it decreased to 1.89 ns in the presence of the dye, indicating the association of GFP:H2B with nucleic acids (Table 2). On the other hand, no significant difference in GFP lifetime was observed for free GFP samples (2.29 ns to 2.30 ns), in the absence or presence of Sytox Orange. Values for control samples are in accordance with our previous reports (Ramirez-Garcés *et al.*, 2016; Camborde *et al.*, 2017). We monitored the association of GFP:MtRH10 with nucleic acids by following the decrease in GFP lifetime in the presence of Sytox Orange. A significant decrease from 2.32 ns to 2.08 ns was observed, as noted in Table 2. Samples were further treated with RNase to check the specificity of the association of MtRH10 with nucleic acids. The results given in Table 2 show that RNase treatment of the GFP:H2B agroinfiltrated samples does not modify the significant decrease in GFP lifetime in the presence of Sytox Orange dye, indicating that GFP:H2B control proteins were associated with DNA. By contrast, there is no significant difference in GFP lifetime in the absence (1.94 ns $\pm$ 0.028) or presence of Sytox Orange (1.95 ns $\pm$ 0.035) in RNase-treated GFP:MtRH10 samples (Table 2). These results indicate that MtRH10 binds plant nuclear RNA.

To determine whether MtRH10 relocalization by AeSSP1256 to the nucleoli rim affects its binding capacity, we performed FRET-FLIM assays to evaluate nucleic acid interactions. A *35S:GFP:MtRH10* construct and a *35S:AeSSP1256:HA* construct were co-expressed in *N. benthamiana* leaves, and the recovery of GFP fluorescence lifetime was monitored 1 d after treatment. Measurements made in nuclei where both tagged-proteins were detected indicated that the GFP lifetime of GFP:MtRH10 remained unchanged, with or without the Sytox Orange acceptor (2.30 ns under both conditions) (Table 3). This assay shows the inability of MtRH10 to bind nucleic acids in the presence of the effector *in planta*.

MtRH10 is expressed in root meristematic tissue and is involved in the development of *M. truncatula* roots

To decipher the function of MtRH10, we first considered its expression by mining public transcriptomic databases PHYTOZOME (https://phytozome.jgi.doe.gov/pz/portal.html), MT EXPRESSV1 (https://lipm-browsers.toulouse.inra.fr/pub/expressionAtlas/app/) and MEDICAGOEFP BROWSER (http://bar.utoronto.ca/efpmedicago/cgi-bin/efpWeb.cgi). No significant variations were detected among the conditions tested in the databases, and no transcriptional changes were detected in our RNA-Seq data generated from *M. truncatula* roots infected by the pathogen, or in qRT-PCR using AeSSP1256-expressing roots (Fig. S6).

By using a MtRH10 promoter-driven GUS (β-glucuronidase) chimeric construct, we detected GUS activity mainly in meristematic cells at the root tip or in lateral emerging roots (Fig. 5a). We then overexpressed a GFP-tagged version of MtRH10 in *M. truncatula* roots. Confocal imaging confirmed the nucleocytoplasmic localization of MtRH10 when compared with GFP-control roots. We observed the accumulation of MtRH10 as brighter dots in the nucleolus of *M. truncatula* cells (Fig. 5b), probably corresponding to the fibrillar centers of nucleoli containing rDNA. No developmental defects were detected in roots

Fig. 5 MtRH10 is expressed in meristematic cells of *Medicago truncatula*, and its deregulation impacts root system architecture (RAS). (a) A 1.44 kb region of the MtRH10 promoter fused to a GUS-encoding gene was transformed into *M. truncatula* roots using *Agrobacterium rhizogenes*. Transformed roots (21 d old) were stained with X-Gluc for 2 h, after which blue colouring, corresponding to MtRH10 promoter expression, was observed. Photographs were taken of the root tip (top panel) and emerging lateral root (bottom panel). Arrows indicate the blue cells. Bar, 100 μm. (b) Representative fluorescence images taken using confocal laser scanning microscopy, of *M. truncatula* roots with a *35S:GFP* (top panel) or *35S:GFP:MtRH10* construct (bottom panel) 21 d after *A. rhizogenes*-mediated root transformation. Note the nucleocytoplasmic localization of GFP:MtRH10, with some brighter dots in the nucleolus (arrows). Lower panels represent the corresponding nucleus enlargements. n, nucleus. Bar, 10 μm. Left panel: 488 nm excitation wavelength; right panel: overlay (488 nm + bright field). (c) Representative photographic images of *M. truncatula* plants transformed at the root level with a *35S:GFP*, *35S:GFP:MtRH10* or *35S:RNAi MtRH10* construct at 21 d after transformation. No particular phenotype distinguished the control GFP roots from those that overexpress MtRH10. Developmental delay was observed in roots compromised for MtRH10 expression (missense MtRH10). Bar, 1 cm. (d) Quantification of root number (top panel) and primary root length (cm; bottom panel) of transformed control roots, *35S:MtRH10* and *35S:RNAi MtRH10* roots at 21 d after transformation. The boxes indicate the interquartile range (25th to the 75th percentile). The central line within the boxes represents the mean value. The whiskers indicate the minimum and maximum values. The jittered data points were superimposed onto the box plot to show the underlying distribution of the data. Results were obtained from three independent experiments for a total of 80 GFP-transformed plants, 55 *MtRH10*-transformed plants and 45 *RNAi:MtRH10*-transformed plants. The lowercase letters ('a' and 'b') indicate significant differences according to Student's *t*-test (where data belong to different classes if $P < 0.01$). (e) Representative longitudinal section of *M. truncatula* root tips transformed with a *35S:GFP* (left) or *35S:RNAi MtRH10* (right) construct. Root apical meristem (RAM) size is determined from the quiescent center (dot line) up to the elongation/differentiation zone (EDZ), defined by the first elongated cortex cell of the second cortical layer (arrowhead). Note the reduced RAM size and the modified shape of EDZ cells in roots in which MtRH10 expression is compromised. Bar, 100 μm. (f) Histograms of total RAM size and mean RAM cortical cell size of the corresponding transformed roots. Note that the RAM of roots in which MtRH10 expression is compromised are smaller than those of GFP control roots, but the average cell size of cortical cells in the RAM is not significantly different. Bars represent mean values and the error bars represent SD. Asterisks indicate a significant difference according to Student's *t*-test (***, $P < 0.0001$; ns, not significant).

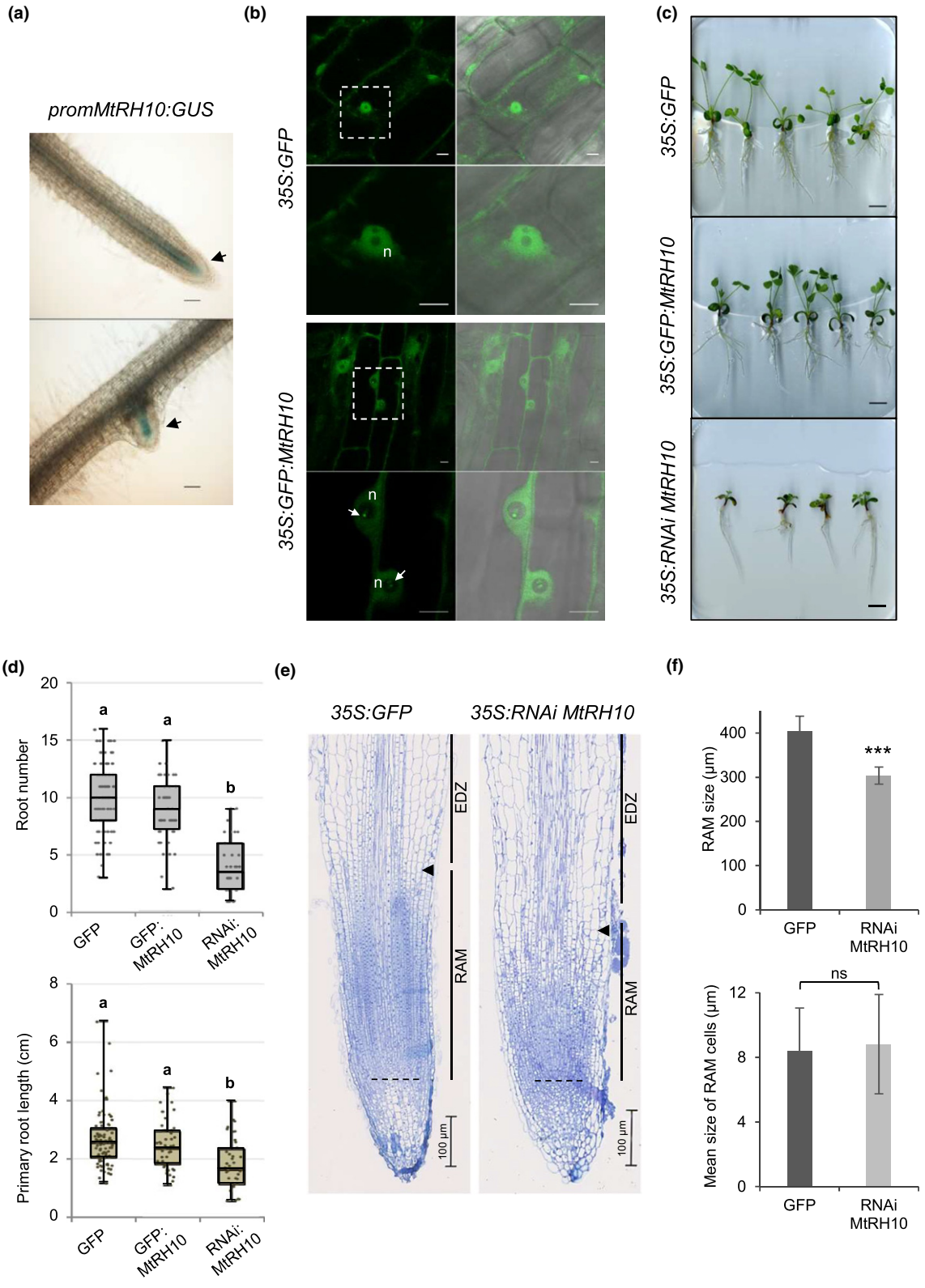

overexpressing MtRH10 (Fig. 5c,d). By contrast, in silenced MtRH10 roots, obtained with a specific 3′UTR region of the MtRH10 sequence (Fig. S7a), we detected a smaller number of roots and a reduced primary root length (Fig. 5c,d). Using qRT-PCR primers that amplified transcripts of MtrunA17_Chr1g0155201 and MtrunA17_Chr6g0483491 in combination with MtrunA17_Chr7g0236841, we confirmed the reduced expression of MtRH10 (by a factor of 3–5) in these transgenic

roots at 21 d post transformation (Fig. S7b), while the expression of MtRH10-related genes was maintained (Fig. S7c).

The reduced expression of MtRH10 triggers nucleoli enlargement in *M. truncatula* root cells, as depicted in Fig. S8(a) and quantified in Fig. S8(b). Longitudinal sections revealed a reduced RAM size in MtRH10 silenced cells, due to a decrease in cortical cell number rather than a smaller cell size (Fig. 5e,f). The cells in the EDZ of these transgenic roots lost their rectangular shape, and their sizes were decreased by a factor of two compared to control roots (Fig. S9). The same developmental defects were detected in roots expressing the AeSSP1256 effector (Fig. S9). The data show that in cell division zones, MtRH10 is associated with *M. truncatula* root development, and AeSSP1256 may affect its activity.

MtRH10 is associated with the ribosome biogenesis pathway and promotes *M. truncatula* tolerance to pathogen infection

To assess whether an impaired MtRH10 initiates nucleolar stress, as suggested by the presence of enlarged nucleoli in silenced MtRH10 roots, we performed qRT-PCR using the same set of primers to confirm this effect in AeSSP1256-expressing roots. As shown in Fig. 6(a), in silenced MtRH10 roots, all 17 ribosome-related genes were downregulated, indicating that MtRH10 is associated with the ribosome biogenesis pathway. Hence, we investigated whether MtRH10 contributes to *M. truncatula* root resistance to the soil-borne pathogen *A. euteiches*. MtRH10 overexpressing and MtRH10-silenced roots were inoculated with zoospores of *A. euteiches*. Western-blot analysis confirmed the presence of MtRH10 at all times of pathogen infection in MtRH10-overexpressing roots (Fig. S10). A reduced amount of mycelium was seen after 7, 14 and 21 d of infection in roots overexpressing MtRH10, compared to GFP-control roots, as shown by qPCR (Fig. 6b). By contrast, transgenic roots in which MtRH10 expression was compromised contained *c.* 5–10 times larger quantities of the pathogen at 7, 14 and 21 d post-infection (Fig. 6c). These assays show that MtRH10 is implicated in basal resistance to *A. euteiches* infection in *M. truncatula*.

Discussion

To modulate host cell processes and facilitate infection, filamentous plant pathogens secrete an array of effector proteins which target various plant components. Here we report that the small protein AeSSP1256 secreted by *A. euteiches* can potentially induce nucleolar stress to promote infection by targeting a host nucleocytoplasmic DExD-box RH (MtRH10) associated with ribosome biogenesis and root development.

Our experiments revealed that transient expression of AeSSP1256 in *M. truncatula* hairy roots triggers developmental defects and facilitates pathogen infection of the partially resistant A17-Jemalong line. This modification to the output of infection is highly relevant, since the quantitative resistance of *M. truncatula* to *A. euteiches* is correlated with root development, and this indicator is strongly correlated with other infection markers such as the death of the plant or the necrosis of cotyledons (Jacquet & Bonhomme, 2020). We have also demonstrated that the detrimental effect of the effector necessitated a localization to the nucleoli rim, showing that the plant nucleolus plays a key role in pathogen resistance.

The nucleolus is a membrane-free subnuclear compartment that is essential for the highly complex process of ribosome biogenesis. The sizes and morphologies of nucleoli are linked to nucleolar activity (Shaw & Brown, 2012). We observed that AeSSP1256 promotes nucleolar expansion of *M. truncatula* root cells. Similar enlargement of the nucleolus, together with excessive accumulation of pre-rRNA processing intermediate has been reported in several Arabidopsis ribosome-related mutants (Ohbayashi & Sugiyama, 2018). Moreover, defects in root development and retarded growth are typical characteristics of Arabidopsis ribosomal protein mutants (Wieckowski & Schiefelbein, 2012; Ohbayashi *et al.*, 2017). In animals, perturbation of any of the steps of ribosome biogenesis in the nucleolus can cause nucleolar stress that is associated with modification of the size and shape of the nucleolus. This in turn stimulates specific signaling pathways, leading, for example, to arrested cell growth (Pfister, 2019).

Considering the localization of AeSSP1256 to the nucleoli rim in combination with nucleoli hypertrophy, we hypothesize that AeSSP1256 most likely causes nucleolar stress by interfering with the host ribosome biogenesis pathway. RNA-Seq experiments showed that within A17-roots, AeSSP1256 downregulated numerous ribosome-related genes. This effect was also detected in susceptible F83005.5 *M. truncatula* lines infected by *A. euteiches*.

AeSSP1256 targets a nucleocytoplasmic DExD/H box RH in *M. truncatula* (MtRH10). The DExD/H box protein family includes the largest family of RHs (Fuller-Pace, 2006). These proteins participate in all RNA processes, including RNA export and translation, and splicing. However, the most common function of these proteins is in ribosome biogenesis, including the assembly process (Jarmoskaite & Russell, 2011). MtRH10 is related to the rice nucleolar RH OsRH10 (TOGR1), which is involved in rRNA homeostasis (Wang *et al.*, 2016), and the *Arabidopsis* nucleolar RH AtRH10, which is involved in ribosome biogenesis (Matsumura *et al.*, 2016; Liu & Imai, 2018). The human nucleolar RH DDX47 (Sekiguchi *et al.*, 2006) and yeast nuclear RH RRP3 (O'Day, 1996) orthologs are parts of a large ribonucleoprotein complex (SSU) that mediates 18S rRNA biogenesis in eukaryotes (Martin *et al.*, 2013; Vincent *et al.*, 2018). Like DDX47, MtRH10 possesses a bipartite nuclear transport domain that can function as an NLS, and two NESs. MtRH10 probably shuttles between the cytoplasm and the nucleus/nucleolus, as has been reported for many other RHs that are involved in rRNA biogenesis and splicing (Sekiguchi *et al.*, 2006; Wang *et al.*, 2009).

Plant genomes encode a large variety of DExD/H RH families, and several are associated with plant development, hormone signaling or responses to abiotic stresses (Liu & Imai, 2018). We show that MtRH10 expression is restricted to the root apical meristematic zone where cells divide. MtRH10 regulates primary

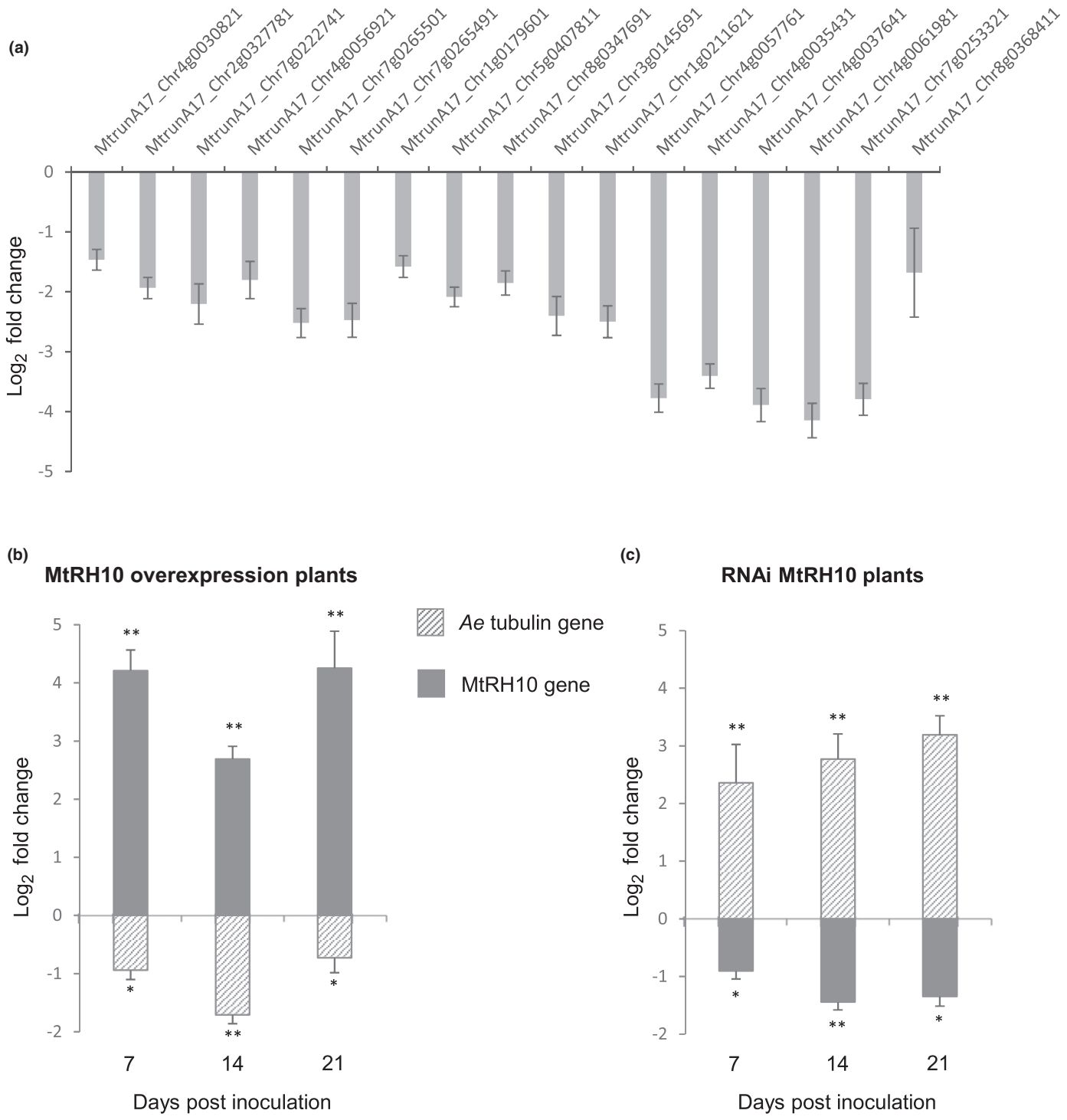

Fig. 6 MtRH10 is a DExD-box RNA helicase that is associated with the ribosome biogenesis pathway and is required for *Medicago truncatula* resistance to soil-borne pathogens. (a) Quantitative reverse transcription polymerase chain reaction (qRT-PCR) analyses for selected ribosome biogenesis-related genes in compromised MtRH10 (RNAi MtRH10) expressing roots compared to green fluorescent protein (GFP) control roots. Note that all these genes were also downregulated in AeSSP1256:GFP expressing roots as reported in Fig. 3(b). Bars and error bars represent, respectively, mean and SE values for two independent experiments. In total, $n = 30$ for GFP roots, and $n = 30$ for RNAi MtRH10 roots. Significant differences were observed for all genes (Student's *t*-test; $P < 0.05$). (b, c) Twenty-one days after root transformation by *Agrobacterium rhizogenes* with 35S:GFP, 35S:GFP:MtRH10 or 35S:RNAi:MtRH10 constructs, infection assays were performed using 1000 zoospores of *Aphanomyces euteiches* per plant. Expression analyses were conducted at 7, 14 and 21 d post-inoculation. Expression values (log_2 fold change) were estimated for *A. euteiches* tubulin or MtRH10 genes in *M. truncatula* infected plants at 7, 14 and 21 d post-inoculation in plants overexpressing GFP:MtRH10 (b), and in MtRH10-compromised (RNAi MtRH10) (c) plants, compared to GFP control roots. Note the enhanced susceptibility to *A. euteiches* infection in roots in which MtRH10 expression is compromised, as well as the reduced incidence of the pathogen in roots in which MtRH10 is overexpressed. Asterisks indicate significant differences according to Student's *t*-test (*, $P < 0.05$; **, $P < 0.01$). Bars and error bars represent, respectively, mean and SE values for three independent experiments. In total, $n = 91$ for GFP roots, $n = 50$ for GFP:MtRH10 roots and $n = 50$ for RNAi MtRH10 roots.

and lateral root development, similar to its orthologs AtRH10 and OsRH10 (Matsumura *et al.*, 2016; Wang *et al.*, 2016). In view of the reduced expression of ribosome-related genes in silenced MtRH10 roots, and enlarged nucleoli, we propose that MtRH10 may be part of the nucleolar stress response in *M. truncatula*.

There have been few reports on how DExD/H RHs are involved in plant responses to pathogens. One example is that of OsBIRH1, which enhances disease resistance against *Alternaria brassicicola* and *Pseudomonas syringae* by activating defense-related genes (Li *et al.*, 2008). Another report concerns the PSR1 effector of *Phytophthora sojae*, which targets a putative plant nuclear DExD/H RH and promotes pathogen infection by suppressing small RNA biogenesis of the plant (Qiao *et al.*, 2015). Here we have shown the involvement of MtRH10 in *M. truncatula* resistance to *A. euteiches*.

This work has revealed that microbial effectors possibly promote infection by triggering plant nucleolar stress, but the precise mechanisms linking the MtRH10-mediated signaling pathway and *M. truncatula* susceptibility require further clarification. How plant cells sense perturbations of the ribosome biogenesis pathway and nucleolar problems also remains unclear (Sáez-Vásquez & Delseny, 2019). However, it seems that AeSSP1256 may act as a stimulus of nucleolar disorder. It is worth bearing in mind that MtRH10 may have functions other than the modulation of nucleolar stress, as exemplified by its ortholog TOGR1 in rice (OsRH10), which mediates adaptation of the primary metabolism required for plant growth at high temperatures by acting as an RNA chaperone (Wang *et al.*, 2016). In addition, the phenotypes of MtRH10-silenced mutant plants and AeSSP1256-expressing plants are very similar to those of auxin-related mutants (Ohbayashi *et al.*, 2017), suggesting that MtRH10 could be directly linked to auxin-regulated morphogenesis in *M. truncatula* roots. Further clarification of which ribosome-related genes, hormones and metabolites cause aberrant root phenotypes would improve our understanding of how defects in the MtRH10-mediated signaling pathway promote *A. euteiches* infection.

In conclusion, we found that soil-borne oomycetes promote disease via small secreted effectors which inhibit plant nuclear DExD/H RHs associated with the ribosome biogenesis pathway and resistance to pathogens. This work provides new insights into plant–root oomycete interactions and also highlights the need for the fine-tuning of plant ribosome biogenesis pathways to successfully combat pathogen infection.

Acknowledgements

The authors would like to thank the GeT-PlaGe genomic platform (https://get.genotoul.fr/en/; Toulouse, France) for RNA-Seq studies, H. San-Clemente and M. Aguilar for help with statistical analysis (LRSV, France), and S. Courbier and A. Camon for their assistance in cloning steps. Editorial assistance from R. Bacsa is acknowledged. The authors would like to thank the reviewers for their insightful suggestions which helped to improve the manuscript. This work was supported by the French Laboratory of Excellence project 'TULIP' (ANR-10-LABX-41; ANR-11-IDEX-0002-02) and by the H2020 European Union's Horizon Research and Innovation program under grant agreement no. 766048 (MSCA-ITN-2017 PROTECTA). The authors declare that they have no conflicts of interest.

Author contributions

LC designed and performed the molecular experiments on AeSSP1256 and contributed to the writing of the manuscript; AK prepared and analyzed the RNA-Seq experiments and contributed to the writing of the manuscript; AJ and LC performed the FRET/FLIM analyses; CP and LC carried out the confocal studies; ALR performed the cross-sectional and longitudinal studies and analyzed the root architecture of the samples; MJCP prepared and analyzed the yeast two-hybrid assay and performed candidate cloning; BD analyzed the data and contributed to the writing of the manuscript; EG conceived, designed, and analyzed the experiments, managed the collaborative work, and contributed to the writing of the manuscript. All authors read and approved the final draft of the manuscript.

ORCID

Laurent Camborde https://orcid.org/0000-0003-3044-7500
Bernard Dumas https://orcid.org/0000-0002-4138-3533
Elodie Gaulin https://orcid.org/0000-0003-0572-8749
Andrei Kiselev https://orcid.org/0000-0003-0737-4921
Aurélie Le Ru https://orcid.org/0000-0002-0236-791X
Michiel J. C. Pel https://orcid.org/0000-0003-1615-5018
Cécile Pouzet https://orcid.org/0000-0002-2464-1940

Data availability

Data that support the findings of this study are openly available in the Gene Expression Omnibus (GEO) (reference number GEO:GSE109500) and the Sequence Read Archive (SRA) (reference number PRJNA631662), and these and all other data are available from the corresponding author (gaulin@lrsv.ups-tlse.fr) upon reasonable request.

References

Alexa A, Rahnenfuhrer J. 2020. *topGO: enrichment analysis for gene ontology.* R package v.2.40.0 [WWW document] URL https://bioconductor.org

Anders S, Pyl PT, Huber W. 2015. HTSeq–a Python framework to work with high-throughput sequencing data. *Bioinformatics* **31**: 166–169.

Badis Y, Bonhomme M, Lafitte C, Huguet S, Balzergue S, Dumas B, Jacquet C. 2015. Transcriptome analysis highlights preformed defences and signalling pathways controlled by the *prAe1* quantitative trait locus (QTL), conferring partial resistance to *Aphanomyces euteiches* in *Medicago truncatula*. *Molecular Plant Pathology* **16**: 973–986.

Badreddine I, Lafitte C, Heux L, Skandalis N, Spanou Z, Martinez Y, Esquerré-Tugayé MT, Bulone V, Dumas B, Bottin A. 2008. Cell wall chitosaccharides are essential components and exposed patterns of the phytopathogenic oomycete *Aphanomyces euteiches*. *Eukaryotic Cell* **7**: 1980–1993.

Boisson-Dernier A, Chabaud M, Garcia F, Bécard G, Rosenberg C, Barker DG. 2001. *Agrobacterium rhizogenes-transformed* roots of *Medicago truncatula* for the

study of nitrogen-fixing and endomycorrhizal symbiotic associations. *Molecular Plant–Microbe Interactions* **14**: 695–700.

Bonhomme M, André O, Badis Y, Ronfort J, Burgarella C, Chantret N, Prosperi J-M, Briskine R, Mudge J, Debéllé F *et al.* 2014. High-density genome-wide association mapping implicates an F-box encoding gene in *Medicago truncatula* resistance to *Aphanomyces euteiches*. *New Phytologist* **201**: 1328–1342.

Bonhomme M, Fariello MI, Navier H, Hajri A, Badis Y, Miteul H, Samac DA, Dumas B, Baranger A, Jacquet C *et al.* 2019. A local score approach improves GWAS resolution and detects minor QTL: application to *Medicago truncatula* quantitative disease resistance to multiple *Aphanomyces euteiches* isolates. *Heredity* **123**: 4.

Camborde L, Jauneau A, Brière C, Deslandes L, Dumas B, Gaulin E. 2017. Detection of nucleic acid–protein interactions in plant leaves using fluorescence lifetime imaging microscopy. *Nature Protocols* **12**: 1933–1950.

Camborde L, Raynaud C, Dumas B, Gaulin E. 2019. DNA-damaging effectors: new players in the effector arena. *Trends in Plant Science* **24**: 1094–1101.

la Cour T, Kiemer L, Mølgaard A, Gupta R, Skriver K, Brunak S. 2004. Analysis and prediction of leucine-rich nuclear export signals. *Protein Engineering, Design and Selection* **17**: 527–536.

Desgroux A, Baudais VN, Aubert V, Le Roy G, de Larambergue H, Miteul H, Aubert G, Boutet G, Duc G, Baranger A *et al.* 2018. Comparative genome-wide-association mapping identifies common loci controlling root system architecture and resistance to *Aphanomyces euteiches* in Pea. *Frontiers in Plant Science* **8**: 2195.

Djébali N, Jauneau A, Carine AT, Chardon F, Jaulneau V, Mathé C, Bottin A, Cazaux M, Pilet-Nayel ML, Baranger A *et al.* 2009. Partial resistance of *Medicago truncatula* to *Aphanomyces euteiches* is associated with protection of the root stele and is controlled by a major QTL rich in proteasome-related genes. *Molecular Plant–Microbe Interactions* **22**: 1043–1055.

Engler C, Youles M, Gruetzner R, Ehnert TM, Werner S, Jones JDG, Patron NJ, Marillonnet S. 2014. A Golden Gate modular cloning toolbox for plants. *ACS Synthetic Biology* **3**: 839–843.

Escouboué M, Camborde L, Jauneau A, Gaulin E, Deslandes L. 2019. Preparation of plant material for analysis of protein–nucleic acid interactions by FRET-FLIM. In: Gassmann W, ed. *Plant innate immunity. Methods in molecular biology, vol. 1991*. New York, NY, USA: Humana, 69–77.

Fliegmann J, Canova S, Lachaud C, Uhlenbroich S, Gascioli V, Pichereaux C, Rossignol M, Rosenberg C, Cumener M, Pitorre D *et al.* 2013. Lipo-chitooligosaccharidic symbiotic signals are recognized by LysM receptor-like kinase LYR3 in the legume *Medicago truncatula*. *ACS Chemical Biology* **8**: 1900–1906.

Förster T. 1948. Intermolecular energy migration and fluorescence. *Annals of Physics* **437**: 55–75.

Fuller-Pace FV. 2006. DExD/H box RNA helicases: multifunctional proteins with important roles in transcriptional regulation. *Nucleic Acids Research* **34**: 4206–4215.

Gaulin E, Jacquet C, Bottin A, Dumas B. 2007. Root rot disease of legumes caused by *Aphanomyces euteiches*. *Molecular Plant Pathology* **8**: 539–548.

Gaulin E, Jauneau A, Villalba F, Rickauer M, Esquerré-Tugayé M-T, Bottin A. 2002. The CBEL glycoprotein of *Phytophthora parasitica* var-*nicotianae* is involved in cell wall deposition and adhesion to cellulosic substrates. *Journal of Cell Science* **115**: 4565–4575.

Gaulin E, Madoui M-A, Bottin A, Jacquet C, Mathé C, Couloux A, Wincker P, Dumas B. 2008. Transcriptome of *Aphanomyces euteiches*: new oomycete putative pathogenicity factors and metabolic pathways. *PLoS ONE* **3**: e1723.

Gaulin E, Pel MJC, Camborde L, San-Clemente H, Courbier S, Dupouy M-A, Lengellé J, Veyssiere M, Le Ru A, Grandjean F *et al.* 2018. Genomics analysis of *Aphanomyces* spp. identifies a new class of oomycete effector associated with host adaptation. *BMC Biology* **16**: 43.

Grefen C, Donald N, Hashimoto K, Kudla J, Schumacher K, Blatt MR. 2010. A ubiquitin-10 promoter-based vector set for fluorescent protein tagging facilitates temporal stability and native protein distribution in transient and stable expression studies. *The Plant Journal* **64**: 355–365.

Haas BJ, Kamoun S, Zody MC, Jiang RHY, Handsaker RE, Cano LM, Grabherr M, Kodira CD, Raffaele S, Torto-Alalibo T *et al.* 2009. Genome sequence and analysis of the Irish potato famine pathogen *Phytophthora infestans*. *Nature* **461**: 393–398.

Hamon C, Coyne CJ, McGee RJ, Lesné A, Esnault R, Mangin P, Hervé M, Le Goff I, Deniot G, Roux-Duparque M *et al.* 2013. QTL meta-analysis provides a comprehensive view of loci controlling partial resistance to *Aphanomyces euteiches* in four sources of resistance in pea. *BMC Plant Biology* **13**: 45.

He Q, McLellan H, Hughes RK, Boevink PC, Armstrong M, Lu Y, Banfield MJ, Tian Z, Birch PRJ. 2019. *Phytophthora infestans* effector SFI3 targets potato UBK to suppress early immune transcriptional responses. *New Phytologist* **222**: 438–454.

He Q, McLellan H, Boevink PC, Birch PRJ. 2020. All roads lead to susceptibility: the many modes of action of fungal and oomycete intracellular effectors. *Plant Communications* **1**: 4.

Jacquet C, Bonhomme M. 2020. Deciphering resistance mechanisms to the root rot disease of legumes caused by *Aphanomyces euteiches* with *Medicago truncatula* genetic and genomic resources. In: de Bruijin F, ed. *The model legume* Medicago truncatula. Hoboken, NJ, USA: John Wiley & Sons, 307–316.

Jarmoskaite I, Russell R. 2011. DEAD-box proteins as RNA helicases and chaperones. *Wiley Interdisciplinary Reviews: RNA* **2**: 135–152.

Kamoun S, Furzer O, Jones JDG, Judelson HS, Ali GS, Dalio RJD, Roy SG, Schena L, Zambounis A, Panabières F *et al.* 2015. The top 10 oomycete pathogens in molecular plant pathology. *Molecular Plant Pathology* **16**: 413–434.

Kim D, Paggi JM, Park C, Bennett C, Salzberg SL. 2019. Graph-based genome alignment and genotyping with HISAT2 and HISAT-genotype. *Nature Biotechnology* **37**: 907–915.

Kosugi S, Hasebe M, Tomita M, Yanagawa H. 2009. Systematic identification of cell cycle-dependent yeast nucleocytoplasmic shuttling proteins by prediction of composite motifs. *Proceedings of the National Academy of Sciences, USA* **106**: 10171–10176.

Li D, Liu H, Zhang H, Wang X, Song F. 2008. OsBIRH1, a DEAD-box RNA helicase with functions in modulating defence responses against pathogen infection and oxidative stress. *Journal of Experimental Botany* **59**: 2133–2146.

Li H, Handsaker B, Wysoker A, Fennell T, Ruan J, Homer N, Marth G, Abecasis G, Durbin R. 2009. The sequence alignment/map format and SAMtools. *Bioinformatics* **25**: 2078–2079.

Liu Y, Imai R. 2018. Function of plant DExD/H-Box RNA helicases associated with ribosomal RNA biogenesis. *Frontiers in Plant Science* **9**: 125.

Livak KJ, Schmittgen TD. 2001. Analysis of relative gene expression data using real-time quantitative PCR and the $2^{-\Delta\Delta CT}$ method. *Methods* **25**: 402–408.

Love MI, Huber W, Anders S. 2014. Moderated estimation of fold change and dispersion for RNA-seq data with DESeq2. *Genome Biology* **15**: 550.

Martin R, Straub AU, Doebele C, Bohnsack MT. 2013. DExD/H-box RNA helicases in ribosome biogenesis. *RNA Biology* **10**: 4–18.

Matsumura Y, Ohbayashi I, Takahashi H, Kojima S, Ishibashi N, Keta S, Nakagawa A, Hayashi R, Saeź-Váquez J, Echeverria M *et al.* 2016. A genetic link between epigenetic repressor AS1-AS2 and a putative small subunit processome in leaf polarity establishment of *Arabidopsis*. *Biology Open* **5**: 942–954.

McGowan J, Fitzpatrick DA. 2017. Genomic, network, and phylogenetic analysis of the oomycete effector arsenal. *mSphere* **2**: 6.

McLellan H, Boevink PC, Armstrong MR, Pritchard L, Gomez S, Morales J, Whisson SC, Beynon JL, Birch PRJ. 2013. An RxLR effector from *Phytophthora infestans* prevents re-localisation of two plant NAC transcription factors from the endoplasmic reticulum to the nucleus. *PLoS Pathogens* **9**: e1003670.

O'Day C. 1996. 18S rRNA processing requires the RNA helicase-like protein Rrp3. *Nucleic Acids Research* **24**: 3201–3207.

Ohbayashi I, Lin CY, Shinohara N, Matsumura Y, Machida Y, Horiguchi G, Tsukaya H, Sugiyama M. 2017. Evidence for a role of ANAC082 as a ribosomal stress response mediator leading to growth defects and developmental alterations in *Arabidopsis*. *Plant Cell* **29**: 2644–2660.

Ohbayashi I, Sugiyama M. 2018. Plant nucleolar stress response, a new face in the NAC-dependent cellular stress responses. *Frontiers in Plant Science* **8**: 2247.

Pecrix Y, Staton SE, Sallet E, Lelandais-Brière C, Moreau S, Carrère S, Blein T, Jardinaud M-F, Latrasse D, Zouine M *et al.* 2018. Whole-genome landscape of *Medicago truncatula* symbiotic genes. *Nature Plants* **4**: 1017–1025.

Pfister AS. 2019. Emerging role of the nucleolar stress response in autophagy. *Frontiers in Cellular Neuroscience* **13**: 156.

Qiao Y, Shi J, Zhai Y, Hou Y, Ma W. 2015. *Phytophthora* effector targets a novel component of small RNA pathway in plants to promote infection. *Proceedings of the National Academy of Sciences, USA* **112**: 5850–5855.

Ramirez-Garcés D, Camborde L, Pel MJC, Jauneau A, Martinez Y, Néant I, Leclerc C, Moreau M, Dumas B, Gaulin E. 2016. CRN13 candidate effectors from plant and animal eukaryotic pathogens are DNA-binding proteins which trigger host DNA damage response. *New Phytologist* **210**: 602–617.

Rau A, Gallopin M, Celeux G, Jaffrézic F. 2013. Data-based filtering for replicated high-throughput transcriptome sequencing experiments. *Bioinformatics* **29**: 2146–2152.

Rey T, Nars A, Bonhomme M, Bottin A, Huguet S, Balzergue S, Jardinaud M-F, Bono J-J, Cullimore J, Dumas B *et al.* 2013. NFP, a LysM protein controlling Nod factor perception, also intervenes in *Medicago truncatula* resistance to pathogens. *New Phytologist* **198**: 875–886.

Sáez-Vásquez J, Delseny M. 2019. Ribosome biogenesis in plants: from functional 45S ribosomal DNA organization to ribosome assembly factors. *Plant Cell* **31**: 1945–1967.

Schornack S, van Damme M, Bozkurt TO, Cano LM, Smoker M, Thines M, Gaulin E, Kamoun S, Huitema E. 2010. Ancient class of translocated oomycete effectors targets the host nucleus. *Proceedings of the National Academy of Sciences, USA* **107**: 17421–17426.

Sekiguchi T, Hayano T, Yanagida M, Takahashi N, Nishimoto T. 2006. NOP132 is required for proper nucleolus localization of DEAD-box RNA helicase DDX47. *Nucleic Acids Research* **34**: 4593–4608.

Shaw P, Brown J. 2012. Nucleoli: composition, function, and dynamics. *Plant Physiology* **158**: 44–51.

Song T, Ma Z, Shen D, Li Q, Li W, Su L, Ye T, Zhang M, Wang Y, Dou D. 2015. An oomycete CRN effector reprograms expression of plant *HSP* genes by targeting their promoters. *PLoS Pathogens* **11**: 1–30.

Stam R, Jupe J, Howden AJM, Morris JA, Boevink PC, Hedley PE, Huitema E. 2013. Identification and characterisation CRN effectors in *Phytophthora capsici* shows modularity and functional diversity. *PLoS ONE* **8**: e59517.

Tabima JF, Grünwald NJ. 2019. *EFFECTR*: an expandable R package to predict candidate RxLR and CRN effectors in oomycetes using motif searches. *Molecular Plant–Microbe Interactions* **32**: 1067–1076.

Tasset C, Bernoux M, Jauneau A, Pouzet C, Briére C, Kieffer-Jacquinod S, Rivas S, Marco Y, Deslandes L. 2010. Autoacetylation of the *Ralstonia solanacearum* effector PopP2 targets a lysine residue essential for RRS1-R-mediated immunity in *Arabidopsis*. *PLoS Pathogens* **6**: e1001202.

Vincent NG, Michael Charette J, Baserga SJ. 2018. The SSU processome interactome in *Saccharomyces cerevisiae* reveals novel protein subcomplexes. *Wiley Interdisciplinary Reviews: RNA* **24**: 77–89.

Wang D, Qin B, Li X, Tang D, Zhang Y, Cheng Z, Xue Y. 2016. Nucleolar DEAD-Box RNA Helicase TOGR1 regulates thermotolerant growth as a pre-rRNA chaperone in rice. *PLoS Genetics* **12**: e1005844.

Wang H, Gao X, Huang Y, Yang J, Liu ZR. 2009. P68 RNA helicase is a nucleocytoplasmic shuttling protein. *Cell Research* **19**: 1388–1400.

Wang S, McLellan H, Bukharova T, He Q, Murphy F, Shi J, Sun S, Van Weymers P, Ren Y, Thilliez G *et al.* 2019. *Phytophthora infestans* RXLR effectors act in concert at diverse subcellular locations to enhance host colonization. *Journal of Experimental Botany* **70**: 343–356.

van West P, Beakes GW. 2014. Animal pathogenic oomycetes. *Fungal Biology* **118**: 525–526.

Wieckowski Y, Schiefelbein J. 2012. Nuclear ribosome biogenesis mediated by the DIM1A rRNA dimethylase is required for organized root growth and epidermal patterning in *Arabidopsis*. *Plant Cell* **24**: 2839–2856.

Wirthmueller L, Asai S, Rallapalli G, Sklenar J, Fabro G, Kim DS, Lintermann R, Jaspers P, Wrzaczek M, Kangasjärvi J *et al.* 2018. *Arabidopsis* downy mildew effector HaRxL106 suppresses plant immunity by binding to RADICAL-INDUCED CELL DEATH1. *New Phytologist* **220**: 232–248.

Xiong Q, Ye W, Choi D, Wong J, Qiao Y, Tao K, Wang Y, Ma W. 2014. *Phytophthora* suppressor of RNA silencing 2 is a conserved RxLR effector that promotes infection in soybean and *Arabidopsis thaliana*. *Molecular Plant–Microbe Interactions* **27**: 1379–1389.

Zhang M, Li Q, Liu T, Liu L, Shen D, Zhu Y, Liu P, Zhou J-M, Dou D. 2015. Two cytoplasmic effectors of *Phytophthora sojae* regulate plant cell death via interactions with plant catalases. *Plant Physiology* **167**: 164–175.

Supporting Information

Additional Supporting Information may be found online in the Supporting Information section at the end of the article.

Fig. S1 AeSSP1256 preferentially accumulates at the nucleolus rim in *Nicotiana benthamiana* cells.

Fig. S2 Nuclear localization of AeSSP1256 is required for its biological activity in *Medicago truncatula* roots.

Fig. S3 Subcellular localization of AeSSP1256 and its putative host targets in *N. benthamiana* leaves.

Fig. S4 AeSSP1256 drives the relocalization of a nucleocytoplasmic host RNA helicase (MtRH10) around the nucleolus in *N. benthamiana* cells.

Fig. S5 Sequence analyses of the MtRH10 DExD-box RNA helicase.

Fig. S6 AeSSP1256 proteins do not alter MtRH10 expression levels in *M. truncatula* roots.

Fig. S7 Expression of MtRH10 is reduced in *M. truncatula*-silenced roots.

Fig. S8 MtRH10-silenced roots displayed enlarged nucleoli.

Fig. S9 *Medicago truncatula* root cell morphology is affected in roots in which MtRH10 expression is compromised or in which the AeSSP1256 effector is expressed.

Fig. S10 Western blot for MtRH10-overexpression roots infected by *Aphanomyces euteiches*.

Table S1 List of primers used in this study.

Table S2 List of putative AeSSP1256 interactors after yeast two-hybrid screening of *M. truncatula* roots infected by the pathogen.

Table S3 RNA-Seq data for *M. truncatula* roots (A17) expressing either the GFP construct or the AeSSP1256:GFP construct.

Please note: Wiley Blackwell are not responsible for the content or functionality of any Supporting Information supplied by the authors. Any queries (other than missing material) should be directed to the *New Phytologist* Central Office.